EXAMINATION OF MICROSTRUCTURAL LIQUID PHASE BEHAVIOR DURING HEAT TREATMENT OF DOPED – LEAD TELLURIDE THERMOELECTRIC MATERIALS

by

SEAN McCOY LANGAN

A thesis submitted to the

Graduate School-New Brunswick

Rutgers, The State University of New Jersey

In partial fulfillment of the requirements

For the degree of

Master of Science

Graduate Program in Materials Science and Engineering

Written under direction of

Professor Dunbar P. Birnie III

and approved by

_____

_____

_____

New Brunswick, New Jersey

October, 2014

ABSTRACT OF THE THESIS

Examination of Microstructural Liquid Phase Behavior during Heat Treatment of Doped-Lead Telluride Thermoelectric Materials

By SEAN McCOY LANGAN

Thesis Director:
Dunbar P. Birnie III

Thermoelectric materials offer a potentially valuable source of energy by converting a temperature gradient to electricity. Recent progress in alloying, doping, and nanostructuring these materials has increased their figure of merit, bringing this technology closer to widespread use. However, the costs associated with processing and questions about fatigue reliability during long-term use could slow the development process. Liquid phase microstructure shapes are critical for sintering; further understanding of these shapes could potentially be used to improve mechanical response and lower overall processing costs. Here we review our progress with respect to the microstructure development of the material depending on heat treatment and composition.

Thermoelectric materials made up of a PbTe/Ag_2Te system were produced by heat treatments aimed at producing a liquid phase in the material. These samples were then examined through scanning electron microscopy, in an attempt to better understand the microstructure and track the liquid phase.

This study was met with mixed results. While the process outlined does seem to produce faster sintering than undoped samples, full densification was not

achieved. Furthermore, though the silver telluride was identified in the sample through the use of backscattering detection and EDS, the desired accuracy in finding the liquid phase was not achieved. However, the silver telluride was found to penetrate the grain boundaries, create secondary phases and form nano-precipitates, a development that is extremely promising as these features could all scatter phonons and raise the figure of merit of the material.

Acknowledgements

An advanced degree in engineering cannot be achieved without the help of many, many people, and I would like to take this opportunity to thank them. First, I would sincerely like to thank Dr. Birnie for all of his guidance and support during this project. He took me in when I had almost no engineering experience, and helped teach me how to be a materials engineer. Thank you Dr. Birnie, for all of your help during this project, I could not have finished it without you. I would also like to thank Dr. Mona Zebarjadi for allowing me to work with her group on the side, and learn much more about thermoelectrics and engineering that does not appear in this thesis, but that I consider invaluable.

I am extraordinarily grateful for the support of John Meiman and the Hammond Lead Company, along with the NSF funded Ceramic, Composite and Optical Materials Center. Believe me when I say I could not have done this without your support.

I would also like to thank my fellow graduate students. My groupmates, Emma, Josh, Brian and Vishnu, you were all enormously helpful. I would also like to thank all the other members of the department who taught me many of the techniques I used: Minh for her assistance with basic powder processing techniques, Sukanya for teaching me about fifty thousand different ways to use the SEM (and for stepping in frequently when I couldn't get it to work), for all the random people in the machine shop who I accosted to teach me how to use the machines, and for Bob, who taught me, well, everything about everything. Special thanks to Brian (again), Bob (again), and Jesse for guiding me in the ways of the grad student, especially

when my funding was in doubt. Also, though he is not a graduate student, Alex Cadar deserves a shout out here. Alex worked very hard, so thanks mate.

The support staff in the department was invaluable. Thank you, Claudia, for always straightening out my registration when I fouled it up (so basically every semester), and Phyllis for her help, especially every time I locked my keys in one of my labs (so basically every week). A special shout-out goes to Michelle, who helped in every way imaginable.

I'm bound to forget some people, so before I do, if you think I should be thanking you, believe me when I say I am. Thank you all.

My friends back home in Chicago, in Boston and here in New Jersey, I love you all dearly, and I am unbelievably blessed that there are too many of you to name here. You all were rocks in times of hardship and you made the joy much sweeter. You made getting work done very, very difficult, and I'm completely okay with that. Next rounds on me guys. Love yah.

To my grandparents, Donna and Bill, who passed away before I could finish. If I grow up to be half the person you two were, I did something right. I love you.

To Annette, for her love and support. I love you Netters.

To my extended family, the Campbells, the Langans, the Ginns, the Butts, the Steinhausers, and so many others. It's a great problem to have, having too many family members to mention. Thank you and I love you all.

To my parents, for their constant support and unyielding love. You, along with Annette, believed in me when I did not believe in myself. How do you thank your parents for all that they have done for you? Are words ever sufficient? I don't

know what to say, except that you all will never know how much you mean to me, and that I'm the luckiest kid in the world. I love you.

Lastly, to God. Thank you for all you have done for me. I couldn't have done it without you.

Preface

Parts of the Introduction (section 1) and the 3-Hour Sample (section 4.5) are from the following paper:

Sean Langan and Dunbar P. Birnie III, "Examinations of Microstructural Liquid Phase Behavior during Heat Treatments of Doped-PbTe Thermoelectric Materials," *Materials Science and Technology Conference and Exhivition 2013*, **4** (2014) 2616-2622.

Table of Contents

List of Figures

1. Introduction

With many traditional means of producing energy becoming less attractive and more costly, the search for alternative ways to provide power has intensified, and one such alternative is thermoelectric materials. Through the Seebeck Effect, thermoelectrics use temperature gradients to transform heat into useable electricity. When a thermoelectric material pair (one n-type and one p-type) are placed in a temperature gradient, the respective majority carriers, electrons and holes, both diffuse from the hot to the cold side of the gradient, completing a circuit and combining to power external systems.

One important thermoelectric material is lead telluride. Lead telluride is an attractive material because it possesses a high figure of merit, as well as excellent chemical properties [1]. However, all thermoelectrics, including lead telluride, possess problems that are preventing their widespread use. Currently, many thermoelectric materials have low efficiency for converting heat to electricity [2]. There are various approaches being used to raise the figure of merit of the material, and therefore the efficiency, such as lowering the thermal conductivity of the material or raising the electrical conductivity; many of these approaches rely on creating phonon-scattering textured microstructures. In addition, new faster processing routes are being investigated, but many of these processing routes are sometimes problematic in terms of capital cost and throughput rate. Some require multiple long annealings that can take more than 70 hours [3], heat treatments over 1200 K [4], and some use processing techniques that would be difficult to adapt to industry, such as spark plasma sintering [5] and hot pressing [6].

Liquid phase sintering is a route that could potentially help to solve some of the problems facing PbTe. From an industrial standpoint, liquid phase sintering is advantageous because the faster diffusion through the liquid allows for shorter processing times and lower temperatures than used for bulk crystal growth. It could also potentially improve the performance of thermoelectrics because in liquid phase sintering there are often precipitates in the grains, which has been shown to lower the thermal conductivity of the material especially on the nanoscale [7], and it produces intergranular second phases, which in some systems have been shown to lower the thermal conductivity [8]. In one earlier study during mechanical alloying of PbSnTe a phase similar to what develops in liquid phase sintering was found [9], and the authors also noticed it in undoped mechanically alloyed PbTe [10]. In one sintering study of undoped PbTe the authors believed under some conditions they were achieving liquid phase sintering [11].

For the present work, a PbTe/Ag_2Te system was chosen to be studied because of a favorable phase diagram for liquid phase sintering [12] as well as previous evidence of numerous precipitates as well as good material performance [13].

2. Background

2.1 Thermoelectric Effect

Thermoelectricity refers to the electricity that can be generated from certain materials when they are exposed to a temperature gradient. There are three separate phenomena that all fall under the umbrella of thermoelectricity: the Seebeck effect, the Peltier effect, and the Thompson effect.

When two conductors or semiconductors are joined, a temperature gradient is applied, electricity is developed and this phenomenon is known as the Seebeck effect. The effect was discovered in 1821 by its namesake, Thomas Seebeck [14]. Thermodynamically, it can be defined as the following (From [15]):

$$dV = S_{(a,b)}dT \qquad (1)$$

Were dV is the Voltage, dT is the temperature gradient, $S_{(a,b)}$ is the Seebeck coefficient, a and b being the two materials that form the junction. S can be defined as the limit as dT approaches zero of dV/dT. The Seebeck coefficient is an important parameter for any thermoelectric material because it plays a key role in defining the figure of merit that measures its effectiveness.

The Peltier effect is the converse effect where heat is generated by passing a current through the same junction that was mentioned before [16]. As with the Seebeck effect, it can be defined thermodynamically (from [15]):

$$dQ_p \propto Idt = \pi_{a,b}I_{a,b} = \pi_{a,b}q \qquad (2)$$

where I is the current, dt is the duration that the current is applied for, $\pi_{a,b}$ is the Peltier coefficient, also known as the Peltier Voltage, and q is the charge. It is the Peltier effect that is harnessed for thermoelectric cooling [14].

The third effect, known as the Thompson effect, was discovered in 1855 and is the heating or cooling that happens when both a temperature gradient and electricity applied to a single thermoelectric material [14]. Thermodynamically, it can be seen that the Thompson effect combines the Peltier and Seebeck effects [15]:

$$\pi_{a,b} = S_{(a,b)}T \qquad (3)$$

$$dQ_T \propto IdtdT = \tau IdtdT = \tau qdT \qquad (4)$$

where T is the temperature in Kelvin, dQ_T is the Thompson heat, dt is the time, and τ is the Thompson coefficient.

2.2 Thermoelectric Device Architecture

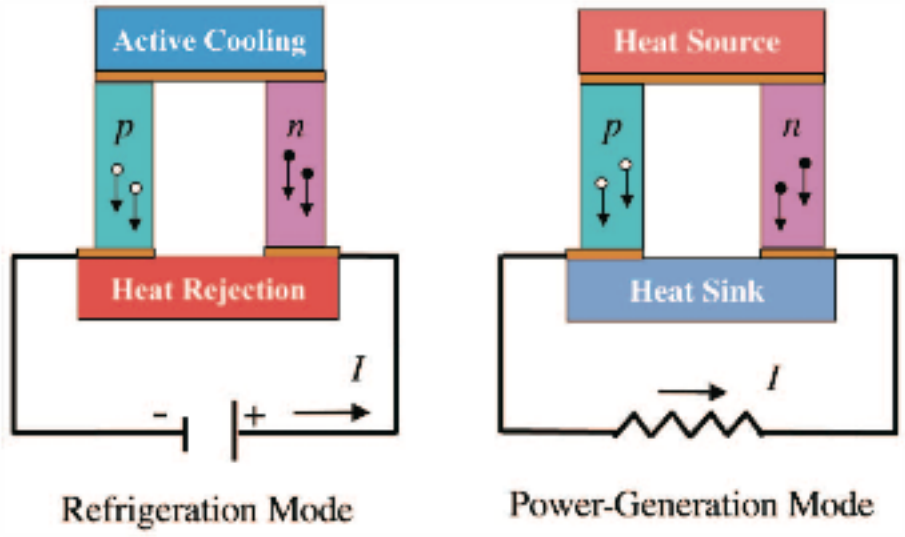

Figure 1: Thermoelectric power generation and cooling. Diagram from [17] showing how holes and charge carriers move with a temperature gradient for both the Seebeck and Peltier effect.

A schematic for a thermoelectric device, or thermoelectric module, is shown in Figure 1. The device consists of "n" and "p" legs, and a "heat source". For thermoelectric power generation (right), the "heat source" and the "cool junction" form a temperature differential across the device. As long as that temperature differential exists, electricity will develop. For thermoelectric cooling (left), electricity is applied to the device, allowing it to absorb heat from one side and dissipate it on the other. Usually thermoelectric devices do not have just one of these "p-n" couples but many, as seen in Figure 2. This is because single

thermoelectric couples produce small voltages at “hundreds of microvolts per degree” [18].

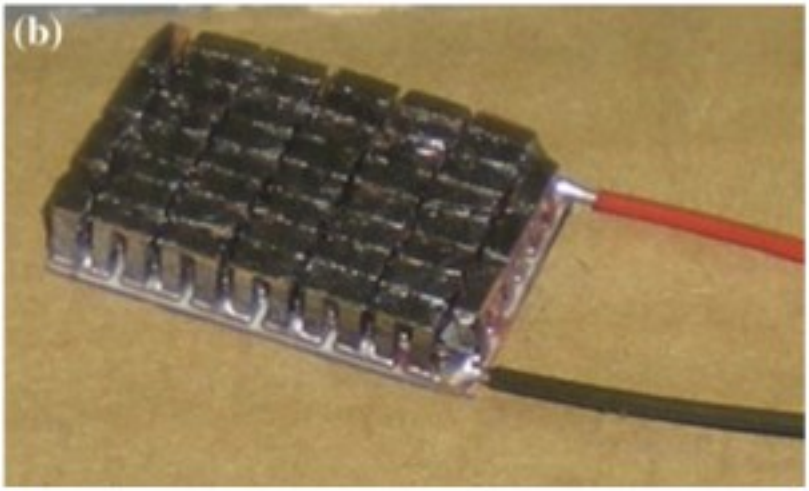

Figure 2 A thermoelectric module. Image from [19] highlighting the high number of thermoelectric legs. A single thermoelectric couple does not produce much power, so many are needed in a single device.

In some cases, it might be possible to construct stacked or composite p-type and n-type sides as shown in Figure 3 [19]. This compensates for the marked temperature dependence of the Seebeck coefficients of different materials and could help improve overall device performance. Here, a lead telluride derivative was used on the “hot” side, and a bismuth telluride derivative was used on the cold side; lead telluride is a better material for hotter temperatures, while bismuth telluride is better for colder temperatures. This distinction comes from the individual figures of merit of the materials (see “Figure of Merit,” section 2.3) and leads to excellent device efficiency. Even though the bismuth telluride derivative only had a figure of merit of approximately 1.2, and the lead telluride derivative had a figure of merit of approximately 1, which are both considered low figures of merit, the efficiency of

the device was found to be 6.56%, and the authors believe that this can be further improved to 9%. This is excellent, and if materials with higher figures of merit can be incorporated into the device this will only serve to further improve the devices' efficiency.

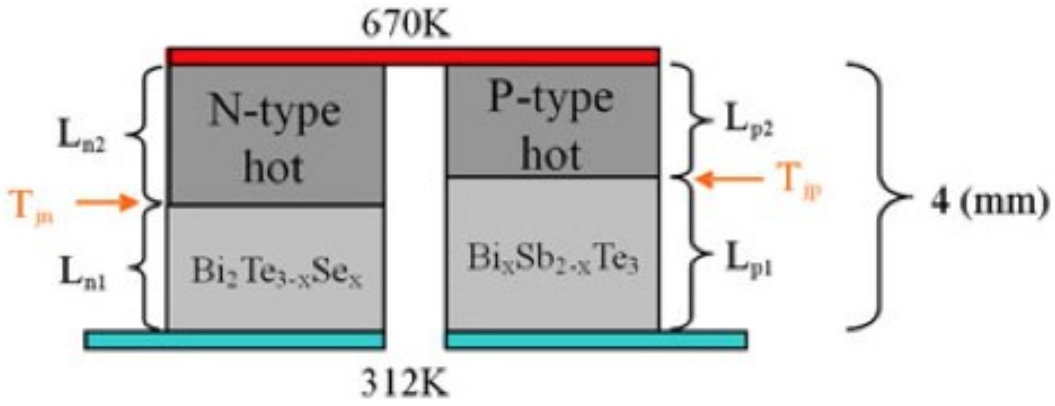

Figure 3: Segmented thermoelectric module. While the device architecture from [19] is more complicated, it allows greater efficiency than a simpler thermoelectric module.

"Functional grading" is also being used to increase the performance of thermoelectric devices [18]. This is when the material is doped in different amounts throughout to coincide with the best doping for the temperature that is likely to apply when in service. This has been successfully done for bismuth telluride by the Bridgman technique. This technique causes a gradient in the carrier concentration in the sample, in turn causing a difference in the properties in the sample from one end to the other. If this technique was successfully used, it could lead to higher efficiencies because each part of the sample would be tailored to its environment.

With work being done to both improve the performance of the thermoelectric materials and improve the overall device, the possibilities for

improving the efficiencies of thermoelectric power generation are exciting and numerous.

2.3 Figure of Merit

Any thermoelectric material's thermoelectric effectiveness can be characterized with a figure of merit (20):

$$\text{Figure of Merit} = ZT = \frac{\sigma S^2 T}{\kappa} \qquad (5)$$

where σ is the electrical conductivity, T is the temperature in Kelvin, S is the Seebeck coefficient, and κ is the thermal conductivity. In order to maximize the figure of merit, a high Seebeck coefficient and electrical conductivity, and a low thermal conductivity are desirable. The researchers in [20] took advantage of this and chose materials with high ZT's at high temperatures for the hot side of their module, and high ZT's at lower temperatures for the cold side of their module. The scientific community is seeking to raise the ZT of known thermoelectric materials, but this is difficult because electrical and thermal conductivities are mechanistically closely related to each other, which usually means that when one is raised, so is the other.

The Seebeck coefficient is the same as is mentioned earlier in this document. It is defined as dV/dT, but can also be defined as "the entropy transported with a charge carrier divided by the carriers charge" [21], and is divided into two components

$$S = S_{presence} + S_{transport} \qquad (6)$$

where $S_{presence}$ "is the change of the net entropy of a solid attendant upon addition of a charge carrier" and $S_{transport}$ "is the energy transported in the transfer process divided by the absolute temperature."

It is often simpler to think of the Seebeck coefficient as the voltage that comes from the change in temperature across the material. Obviously, the more voltage that comes from the temperature gradient, the better the material is. However, this is not the only thing that affects the performance of a thermoelectric material, as the electrical and thermal conductivities also have an effect.

The electrical conductivity of a material is defined as

$$\sigma = \frac{1}{\rho} \qquad (7)$$

where ρ is resistivity of a material. A high electrical conductivity means that charge carriers will have an easier time moving through the material, which allows the voltage that is being generated through the Seebeck effect to be delivered to the load that it is powering. The resistivity of a material is defined as [22]

$$P = \frac{E}{J} = \frac{VA}{Jl} \qquad (8)$$

where E is the electrical field, j is current density, V is change in potential, A is the area of the sample, l is the length of the sample and J is the total current in the sample. The conductivity then would be:

$$\sigma = \frac{j}{E} \qquad (9)$$

A little analysis here reinforces the idea that a high conductivity is valuable. In powering a device, it is desirable to have a large current density over a small change in potential, which coincides with a large current.

A good thermoelectric material also requires a low thermal conductivity. Thermal conductivity is made up of two parts, seen below:

$$\kappa = \kappa_e + \kappa_l \qquad (10)$$

where κ_e is the electronic term of thermal conductivity, and κ_l is the lattice term. The electronic term represents the heat associated with the movement of electrons and electron holes, while the lattice term is for "phonons travelling through the lattice" [23]. Most efforts to lower the thermal conductivity of a material concentrate on the lattice term, since the electrical term of thermal conductivity is proportional to the electrical conductivity of the material through the relationship [23]

$$\kappa_e = L\sigma T \qquad (11)$$

L being the Lorentz factor. Because the electrical conductivity is proportional to the electrical term of thermal conductivity, raising one raises the other, so most efforts are devoted to lowering the lattice thermal conductivity, which is not connected to the electrical conductivity.

Material selection for thermoelectrics based off the figure of merit is difficult as well, and this difficult tradeoff is seen in Figure 4

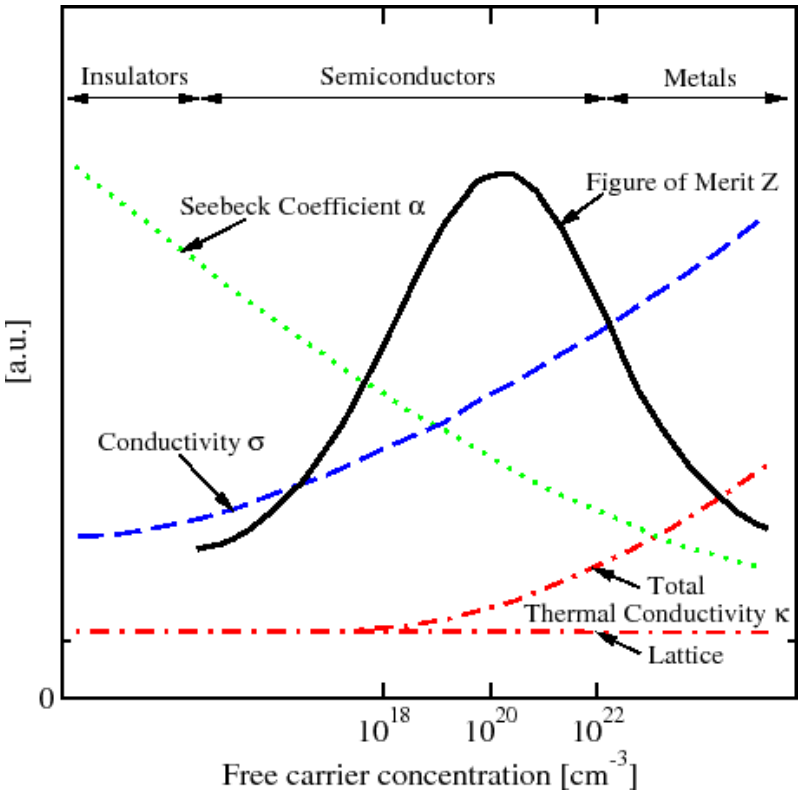

Figure 4. Thermoelectric properties of various materials. A complex tradeoff exists in designing a thermoelectric material. As shown, it is impossible for a material to possess the most desirable performance for all components of the figure of merit, so the engineer must balance the three properties. Figure from [24].

Figure 4 does a good job of illustrating the difficulty in maximizing the figure of merit of a material. Insulators have favorably low thermal conductivity, and an extremely high Seebeck coefficient, but the price is a very low electrical conductivity. The material is not conductive enough to effectively move the current generated to the load. Conversely, metals have a high electrical conductivity, but higher thermal conductivity and a lower Seebeck coefficient. While all materials experience the Seebeck effect to some extent, it is very low for metals making them less useful as thermoelectrics.

Semiconductors have been found to be a happy medium. While they do not possess the highest values of Seebeck coefficient and electrical conductivity, they possess high enough values of both to make for a good thermoelectric material.

2.4 Raising the Figure of Merit

Though the Figure of Merit of a thermoelectric material is well understood, it is important to raise that Figure of Merit as much as possible. Common thermoelectrics have a figure of merit around or lower than one, while it is generally accepted that the number that would produce efficient thermoelectrics is 3 [2]. Efforts at raising the figure of merit focus on improving all aspects, including the Seebeck coefficient, the electrical conductivity, and the thermal conductivity.

While not as much effort is put into raising the Seebeck coefficient as is into bettering the other thermoelectric parameters, it is nonetheless a valuable tool in raising the figure of merit of a material. In one paper the Seebeck coefficient was improved by a factor of 4 at low temperatures, as seen in Figure 5 [25].

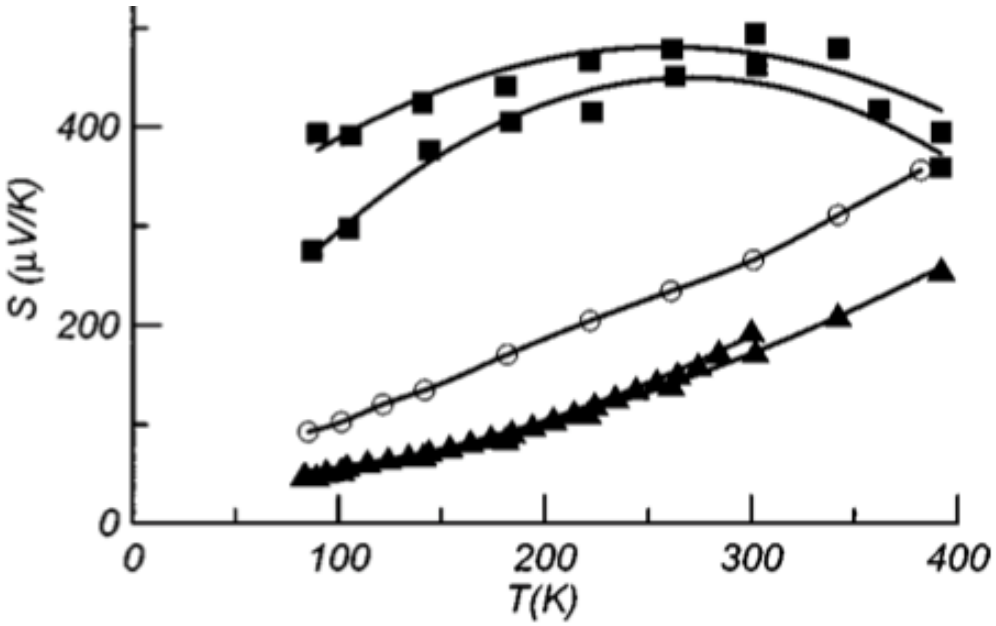

Figure 5: Nanostructurings effect on Seebeck coefficient. The open circles are the baseline lead telluride sample, and the other samples were nanostructured. Nanostructuring allows for great gains in the Seebeck coefficient of a material. Figure from [25].

The group theorized that this increase seen in Figure 5 is from an increase in what they call the "scattering parameter," which in turn increases the Seebeck coefficient. This scattering parameter is related to the density of states in the system. The authors posit that this causes more electron scattering, which raises the thermopower of the system by separating high and low energy electrons.

Improving the electrical conductivity of a sample usually requires doping. Doping a material can increase in the number of charge carriers, which can increase the electrical conductivity of the material. Since the electrical conductivity and part of the thermal conductivity are tied together by the Lorentz factor, the two do need to be carefully balanced, but doping remains an invaluable aspect in creating high performance thermoelectrics.

Lowering the thermal conductivity is mostly centered around scattering phonons, the lattice vibrations responsible for heat conduction. If phonons are able to move unobstructed through a material, it will have a high thermal conductivity.

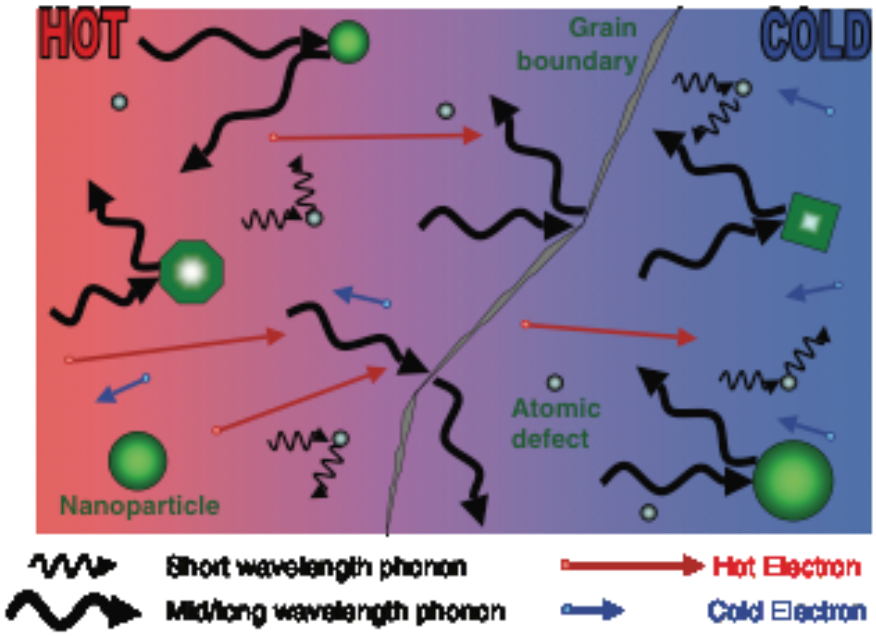

Figure 6: Phonon scattering. A schematic from [7] highlighting that different energy phonons may require different sized scattering features

Different wavelengths of phonons require different sized obstructions to hinder their path through a material, as seen in Figure 6. Small wavelength phonons can be scattered by small microstructural features, such as atomic defects [7]. Phonons with a longer wavelength require larger features, such as grain boundaries or nanoparticles.

This knowledge was used in [26] to engineer a high performance PbTe-SrTe sodium doped thermoelectric. Since phonons of various wavelengths are scattered by differing microstructural features, the material was designed to have features on

the atomic scale, the nanoscale and the mesoscale, seen in Figure 7, leading to a figure of merit of 2.2, one of the highest ever achieved.

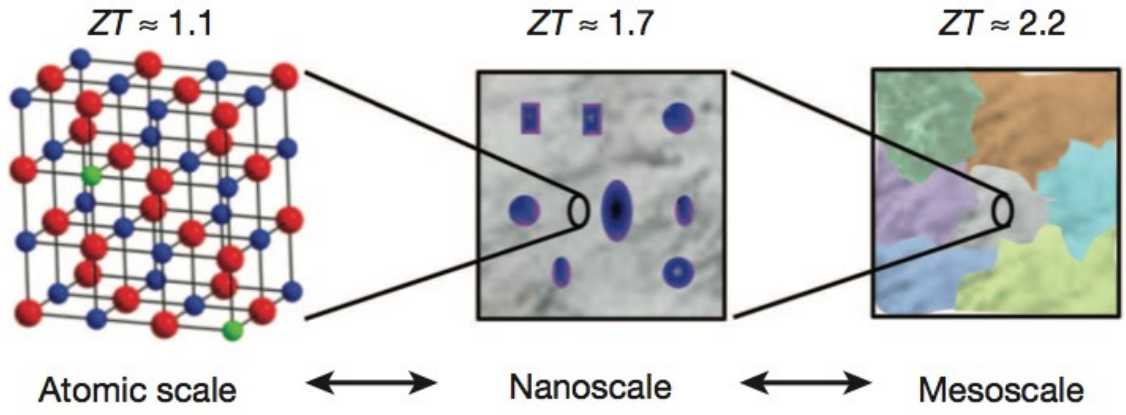

Figure 7: Feature sizes in raising the figure of merit. A diagram of atomic substitutions, nanostructures, and grains and the performance bonuses they provide. Figure from [26].

A mixture of large and small grain sizes was used in [27] (reported in [28]) to raise the figure of merit. In this study, the fraction of "fine" or smaller particles vs "coarse" or large particles was varied.

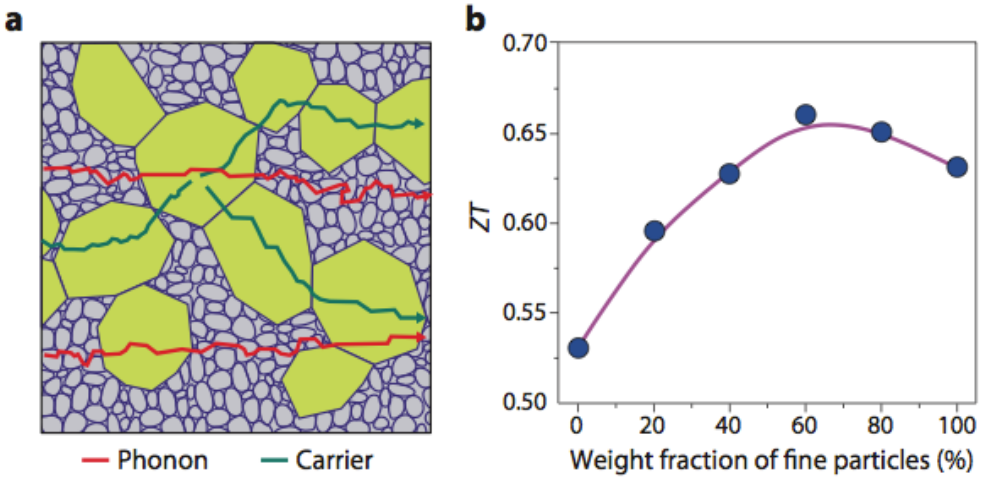

Figure 8: The effect of mixed grain sizes in thermoelectrics. A diagram from [28] showing the paths that carriers and phonons take through a material with mixed grain sizes, and the resulting thermoelectric boost.

It was found that a mixture of large and small grains, rather than exclusively large or exclusively small, yielded the highest figure of merit. This is believed to be because the charge carriers will travel along the large grains, which have the highest conductivity, thus raising the electrical conductivity, while the phonons travel indiscriminately through the sample, lowering the lattice thermal conductivity and thus the overall thermal conductivity. If the ratio of grain sizes is correctly found, it allows for enough of an increase in the electrical conductivity, with a relatively small increase in the thermal conductivity by comparison. Improving the figure of merit of a material almost always involves a tradeoff like this, finding the right balance between competing properties, to improve the overall device

2.5 Literature Review of Current Production Methods

2.5.1 Alloying

Alloying by combining 2 different samples has been proven to be an effective way to raise the figure of merit of a thermoelectric. In 2011, Kim *et al* studied a PbTe-Bi_2Te_3 system [29] because Bismuth telluride is known to be effective at lower temperatures, were lead telluride is not. The compound was synthesized by melting at high temperature, then quenching it. The resulting material had distinct phases, as is evident in Figure 9.

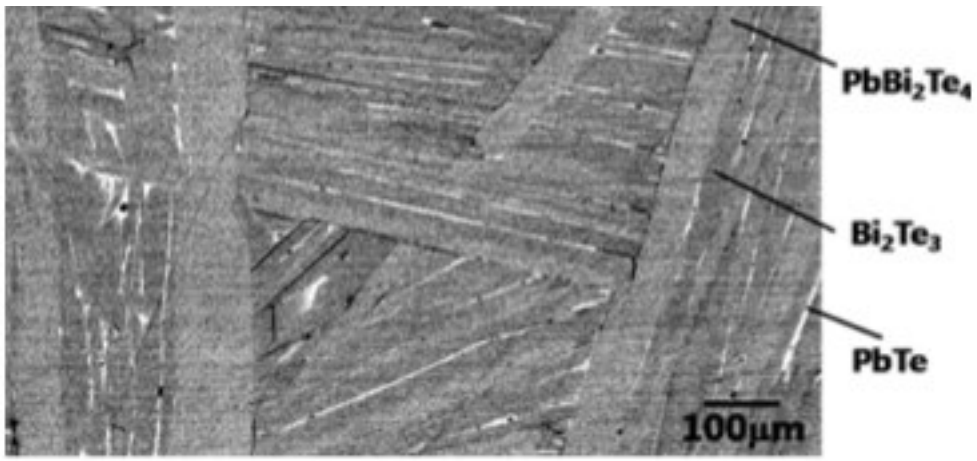

Figure 9: PbTe-Bi_2Te_3 Microstructure. Alloys show a complex microstructure. Figure from [29].

When the alloy was formed this way the two phase microstructure lowered the electrical conductivity, but also decreased the thermal conductivity, again showing the difficulty in improving the figure of merit of a compound.

In a paper from Zhang *et al.* [30] lead telluride had tin ions introduced via ion implantation at room temperature and was then annealed for an hour. Using XRD and XPS it was shown that this process made a material with "graded interfaces between $Pb_{1-x}Sn_xTe$ and PbTe substrate" [30]. These layers raised the electrical conductivity and the Seebeck coefficient, and lowered the thermal conductivity, raising the figure of merit by more than 25%.

Recently a group from Northwestern University was able to discover two new PbTe alloyed systems, PbTe/CaTe and PbTe/BaTe, both doped with Na_2Te [31]. Both of these systems are found to develop precipitates upon being cooled from above the melting point, which is a valuable feature in a thermoelectric material, and is shown in Figure 10.

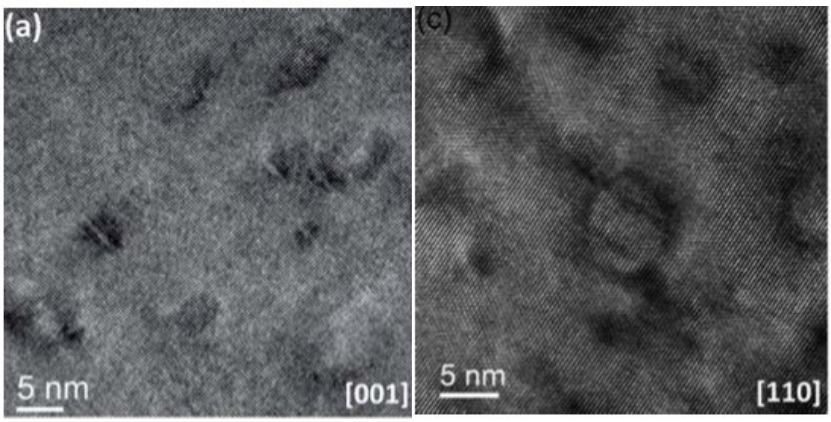

Figure 10: PbTe/CaTe and PbTe/BaTe microstructures. On the left is PbTe alloyed with CaTe and on the right is PbTe alloyed with BaTe. Both show high degrees of nanostructuring, which contributes heavily to phonon scattering. Figure from [31].

The study drew the conclusion that these nanostructures lowered the thermal conductivity of the material, which led to a high figure of merit, seen in Figure 11.

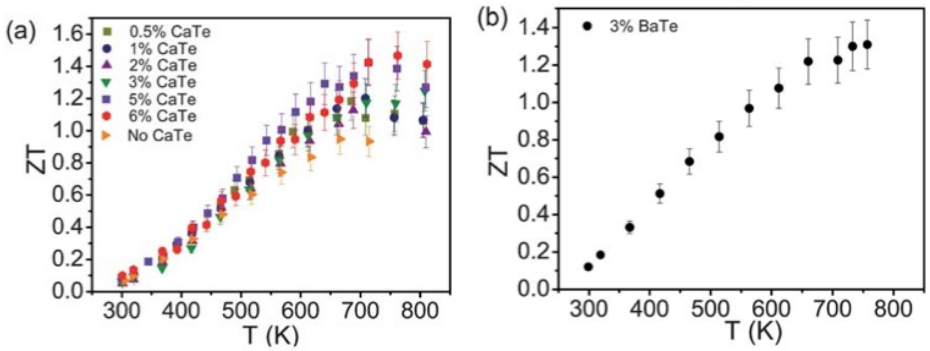

Figure 11: Effect of microstructure on thermoelectric properties of PbTe/CaTe and PbTe/BaTe. On the left is the ZT data from PbTe/CaTe and on the right is the data from PbTe/BaTe. While the PbTe/CaTe system shows greater values, both samples show large improvement over a non-alloyed sample. Figure from [31].

It is worth noting that different levels of CaTe lead to the figure of merit for the alloy to peak at different temperatures. This has potential to be useful for industry, since in an industrial setting it is easier to vary the amount of CaTe to adjust the material for different applications, rather than using different materials for different applications.

In 2010 a group from France took advantage of the miscibility gap of the PbTe-GeTe system to lower the thermal diffusivity of the compound [8] (thermal diffusivity is closely related to the required coefficient, the thermal conductivity).

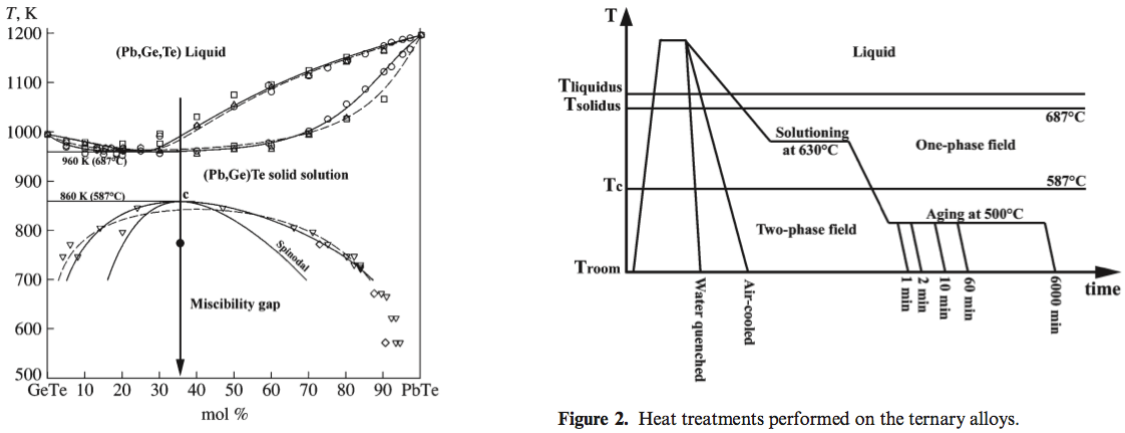

Figure 12: The phase diagram and experimental diagrams for PbTe/GeTe alloys. While all samples stayed in the pure liquid and solutionizing for states the same amount of time, they were allowed to age in the miscibility gap for different amounts of time. Figure from [8].

The PbTe-GeTe system includes a miscibility gap (as seen in Figure 12) that the material was allowed to anneal in for various amounts of time (Figure 1), and depending on the amount of time that a material was allowed to anneal for, very different microstructures formed, as seen in Figure 13. This location within the miscibility gap is susceptible to phase separation via a spinodal decomposition process, which is known to give extremely small microstructural features.

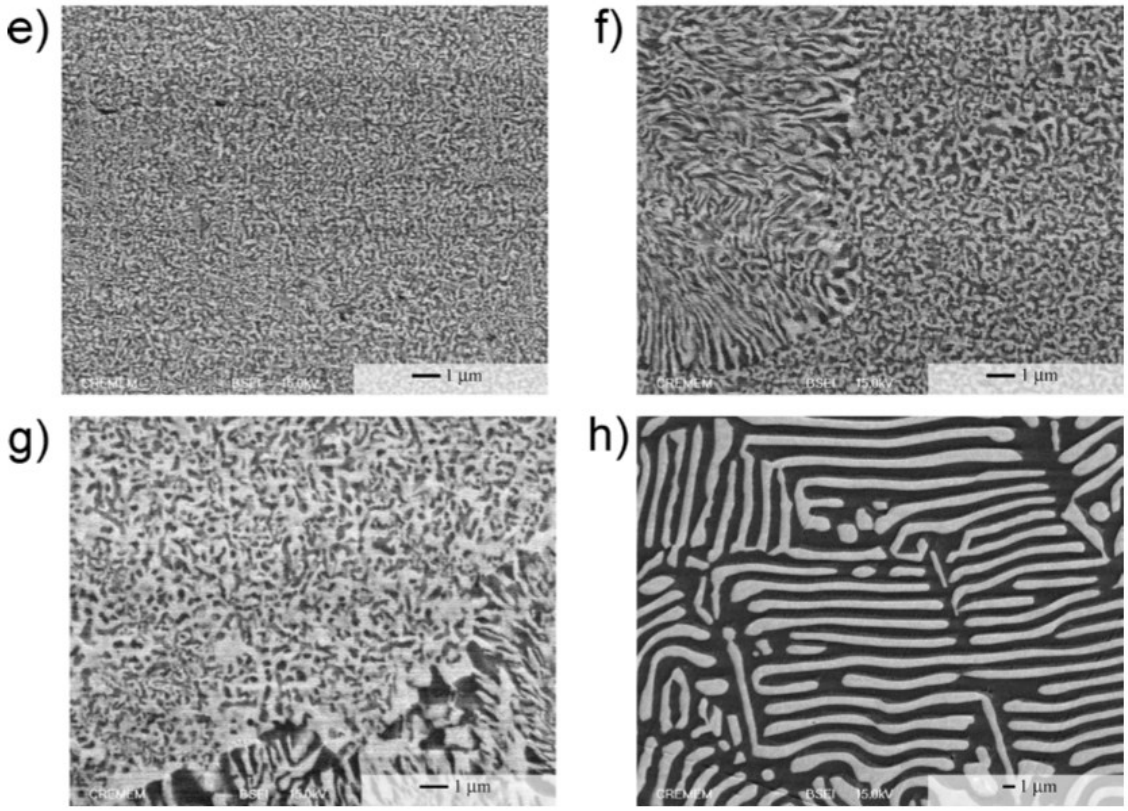

Figure 13: Microstructures of PbTe/GeTe alloys. Samples from [8] annealed for 2(e), 10(f), 60(g), and 6000 (h) minutes. The longer the annealing, the larger the microstructural features in the sample. Figure from [8].

When these samples were tested for thermal diffusivity, it was found that the lowest thermal diffusivity is for the sample annealed for 1 minute.

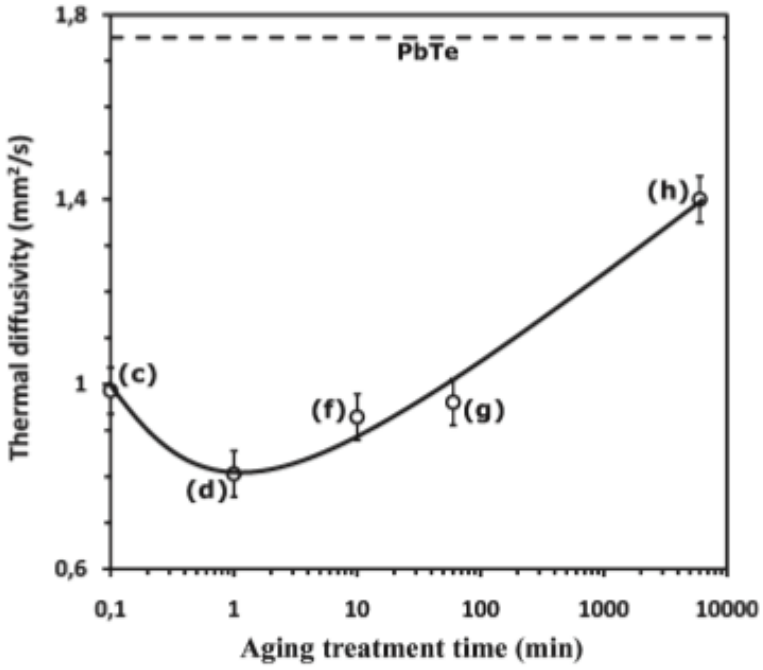

Figure 14: Thermal diffusivity plotted against time for PbTe/GeTe alloys. The lowest diffusivity corresponds to the shortest time ageing. Figure from [8].

Though all the samples have a lower thermal diffusivity than unalloyed lead telluride, the one that is allowed to anneal for the shortest amount of time has the best properties. The authors speculate that this is because the smaller feature sizes on the sample that was allowed to anneal for a shorter period of time allow for better scattering of phonons, which lowers thermal diffusivity. This is useful because long annealing times are unattractive to industry and if this could be exploited in other systems similar results could possibly be obtained.

2.5.2 Doping

Doping is one of the most effective ways to change the thermoelectric properties of a material, and, depending on how it is done, it can be a relatively

simple procedure. In a study by Ao *et al* [32], lead telluride was doped with Cesium. The synthesis was very similar to that of pure lead telluride, in that all the components were melted, ball milled and sintered using SPS.

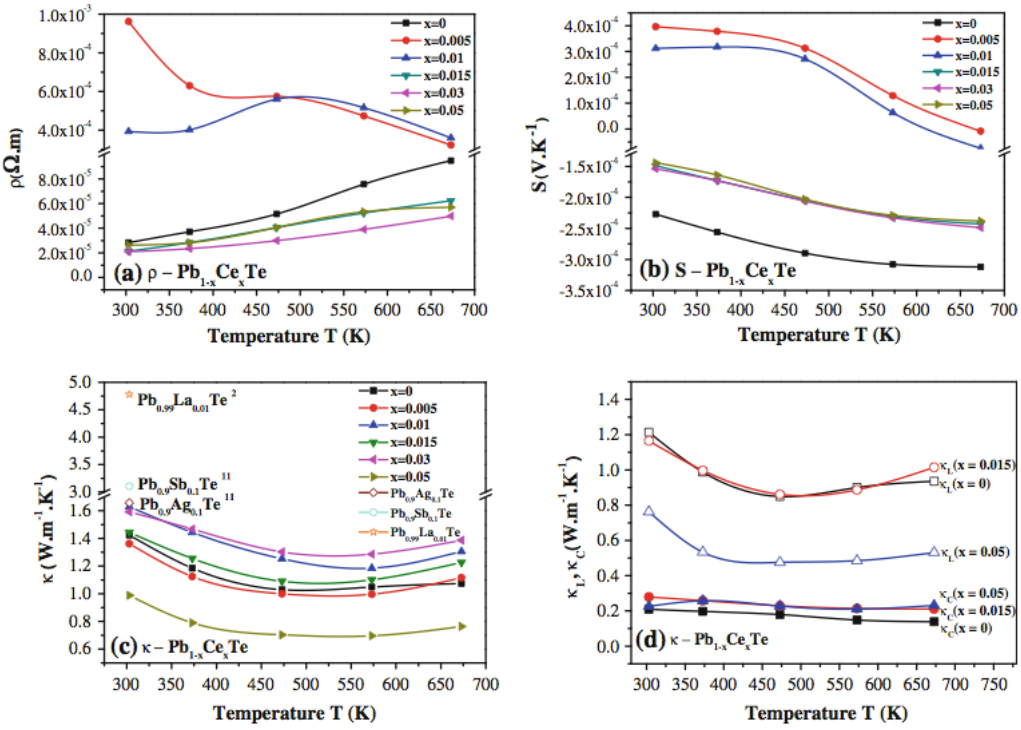

Figure 15: Thermoelectric properties of lead telluride doped with cesium. Graphs of temperature vs (from top left clockwise) electrical resistivity, Seebeck coefficient, thermal conductivity and carrier thermal conductivity. Figure from [32].

As seen in Figure 15, how the amount of doping matters. For example, the material doped with 0.03 atomic percent cesium has the best electrical conductivity, but the highest thermal conductivity. However doping with 0.05 atomic percent raises the figure of merit by more than .2 (as seen in Figure 16).

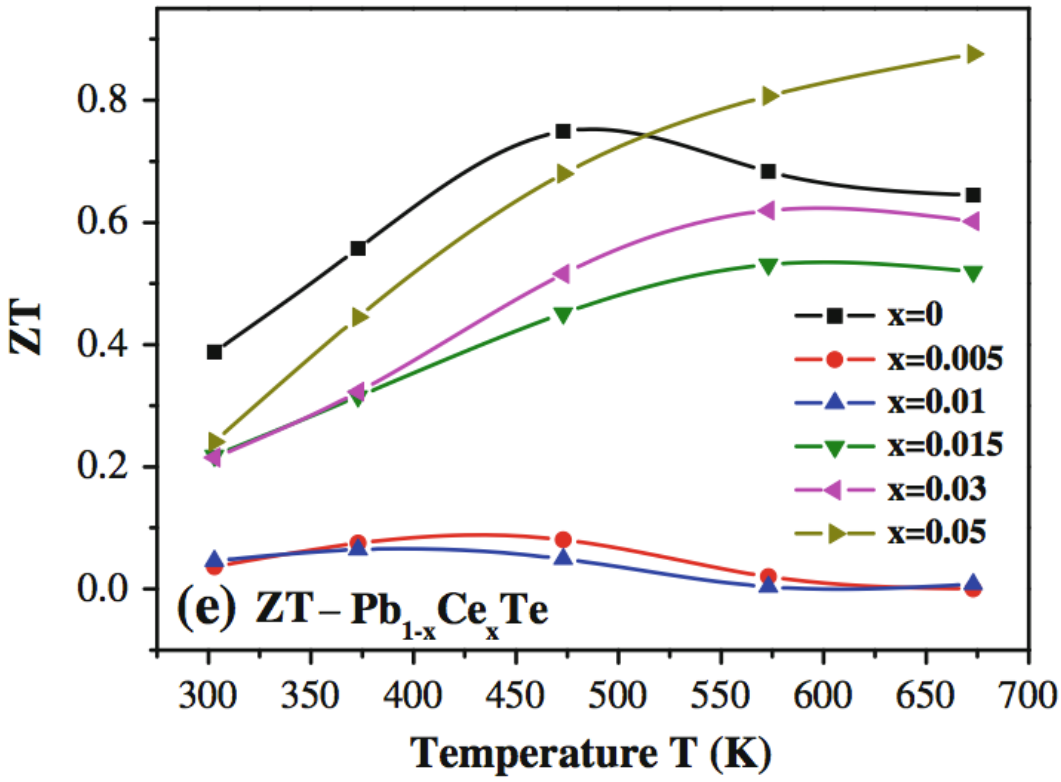

Figure 16: Graph of figure of merit for Ce- doped and undoped lead telluride. Figure from [32].

Doping here allows for a good gain in the electrical conductivity, though it decreases the Seebeck coefficient. However, at higher cesium concentrations a Ce_3Te_4 phase forms which scatters phonons and lowers the thermal conductivity of the material. Doping is clearly a balancing act. The concentrations of the dopant have to be exact, otherwise it will not improve the material.

One of the best results with doping was achieved with codoping by the Mercouri Kanidis of Northwestern University [33]. The sample was prepared as an ingot by melting and cooling the material. The study found that doping the sample with both sodium and potassium gives a figure of merit with a value of 1.3, as seen in Figure 17.

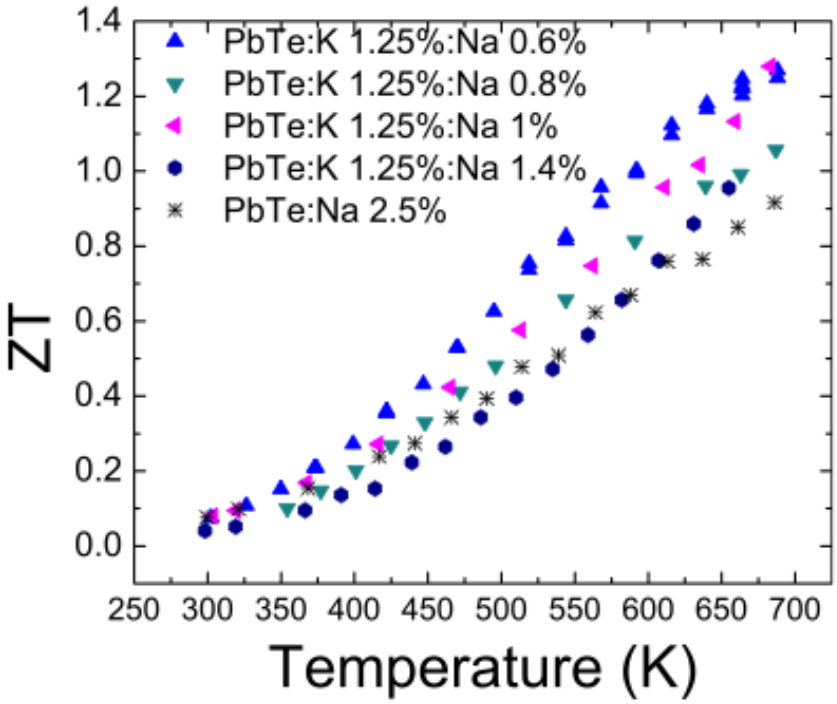

Figure 17: Figure of merit values for potassium and sodium doped lead telluride. Figure from [33].

It was found that the potassium doping changed the "heavy-hole" valence band of the material, and doping with sodium adjusted the Fermi level of the material. These effects, according to the authors, enhance the figure of merit "purely on account of the enhancement in electronic properties and without a marked reduction in thermal conductivity". This could potentially be exploited to further increase the figure of merit by combining it with an approach that decreases the thermal conductivity without markedly changing the electrical conductivity.

2.5.3 Powder Advances

Several techniques have arisen to create a finer powder that can be used when synthesizing the PbTe sample. In [34] it was found that the powder could be made finer with the use of a laser. The starting material was synthesized traditionally, broken with a mortar and pestle into powders ranging from 20 – 100 micrometers, then suspended in water.

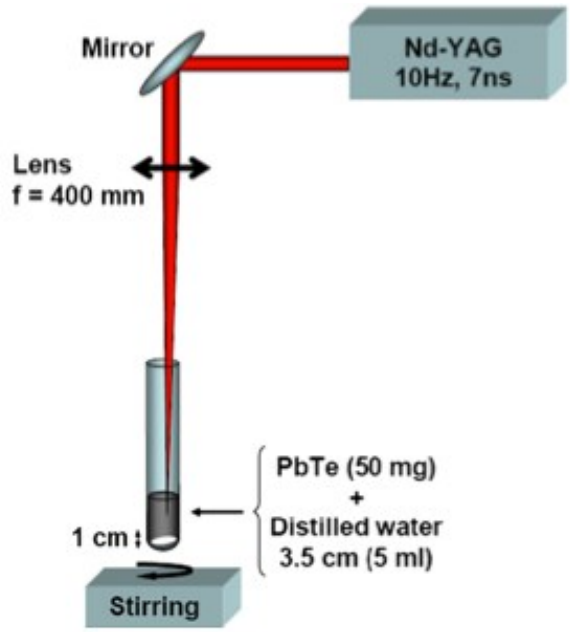

Figure 18: Setup to reduce particle size via laser. The stir bar provided constant stream of particles to the surface to ensure maximum fragmentation. A focal point of 1cm above the bottom of the test tube was found to provide the best results. Figure from [34].

When the powder was subjected to 5 minutes of a laser at 400 mJ, the particle size being reduced to approximately 4-10 nm, as shown in Figure 19.

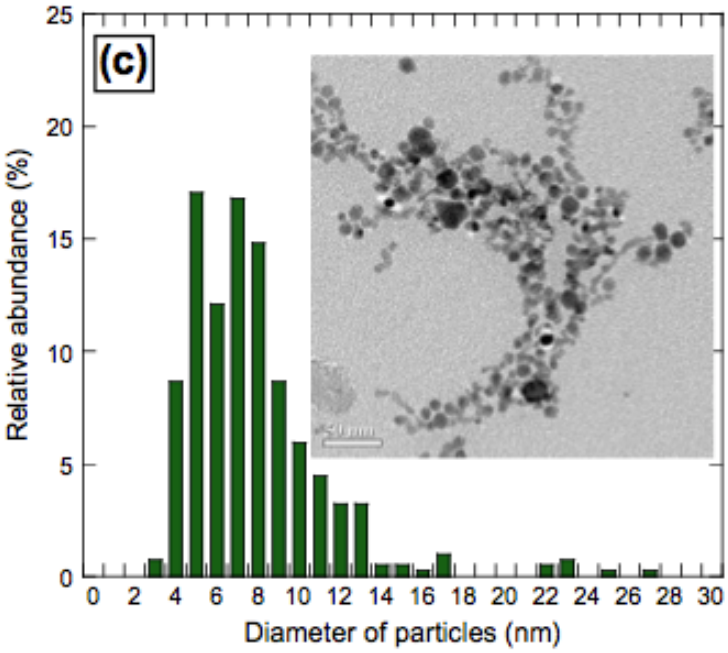

Figure 19: TEM and particle size distribution from laser particle size reduction. Aside from a few above 20nm, the distribution is good. Figure from [34].

This represents a fast method to reduce particle size, however, the authors admitted that it is low yield and only suitable for small batches.

Brock *et al* [35] found it possible to synthesize aerogels and gels of lead telluride. The synthesis did not require temperatures over 170°C, though it did require about a week overall. However, the process gave small powder sizes as demonstrated in Figure 20. The extremely small powder sizes are promising, particularly in areas where a sol-gel method of production is preferable.

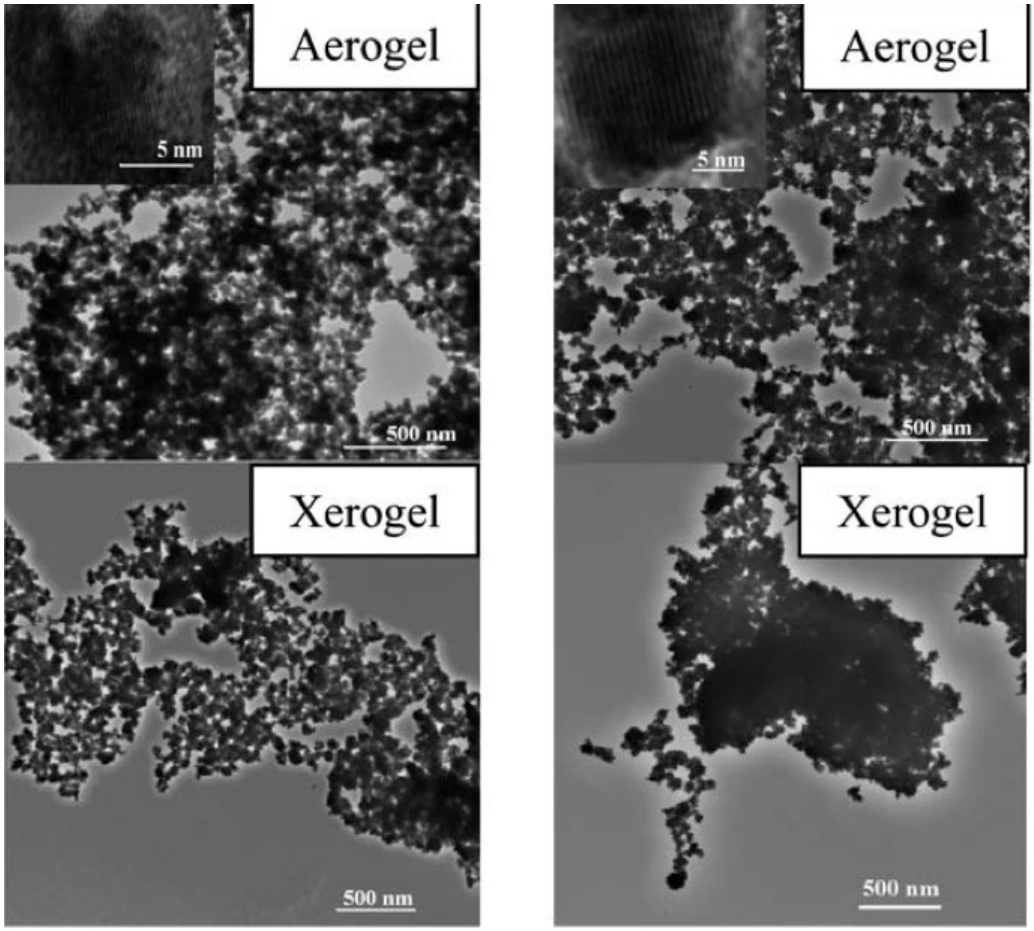

Figure 20: TEM's showing the resulting nanoparticles from laser particle size reduction. The particles exhibit a high degree of agglomeration. Figure from [35].

2.6 Liquid Phase Sintering

Traditional solid phase sintering is the consolidation of a powder into a dense body during a heat treatment. Its driving force is a reduction in the surface energy associated with the powder. It is a common technique to form ceramics due to their high melting points, but is also used for metals and even some polymers.

Liquid phase sintering is different because it occurs in a part of the phase diagram that contains a liquid as well as a solid phase, meaning that there is a liquid present during sintering. This is often from a eutectic system [36]. Liquid phase sintering has a fundamentally different driving force from solid state sintering, because there are three different surface energies competing, though the overall surface energy reduction remains important. When a liquid is in contact with a pore, it generates a pressure on the pore, which can be described by the Young-Laplace equation [36] $\Delta p = -\frac{2\gamma_{lv}}{r}$ (12). This pressure can be large, and can drive the densification of the system. Liquid phase sintering can also enhance the rate of sintering (vs solid state) through "enhanced rearrangement" and "enhanced matter transport" [36]. The liquid phase reduces the friction between the powder grains, allowing for "easier rearrangement" and "Enhanced matter transport" because there is much faster diffusion in a liquid than in a solid.

Liquid phase sintering typically occurs in 3 stages: rearrangement, solution-precipitation, and densification all of which are illustrated in Figure 21.

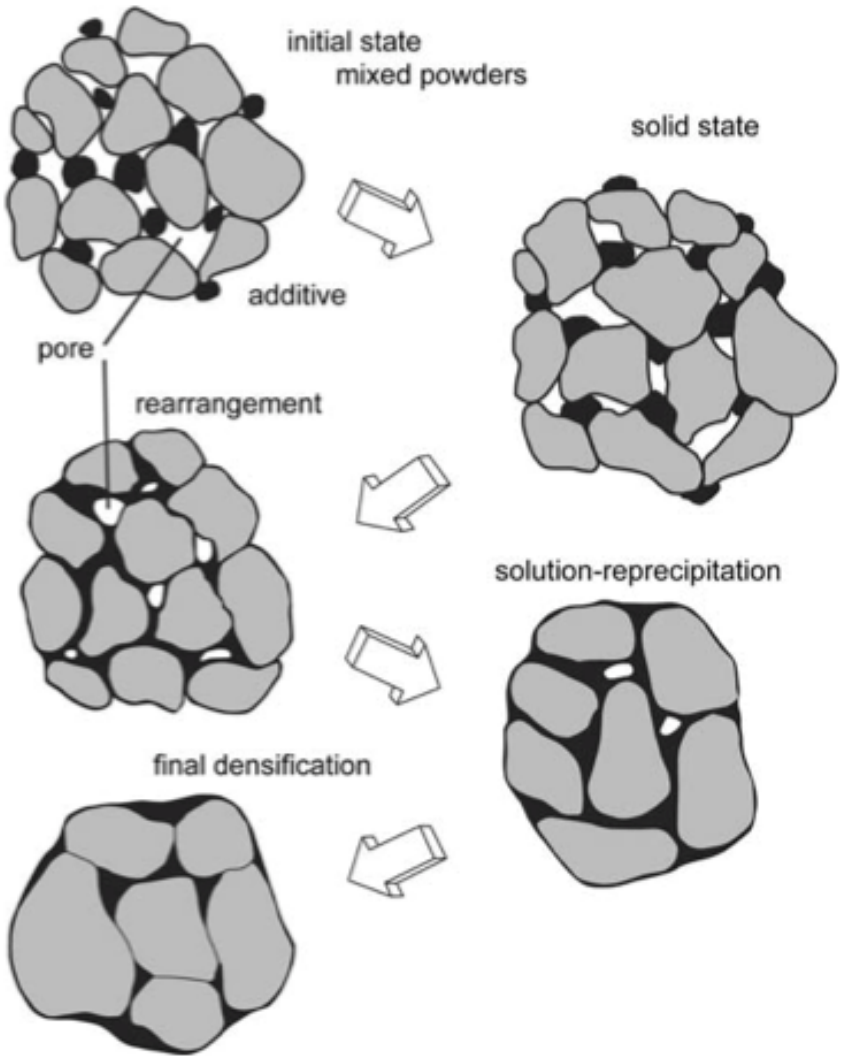

Figure 21: Phases of liquid phase sintering. While the phases are similar to that of solid state sintering, the liquid phase makes for a more complicated process. Figure from [37]

Rearrangement is the first step in liquid phase sintering [36]. A liquid forms, and exerts a pressure on the material causing the powder particles to rearrange themselves to lower the pressure, and any gaps between the particles are filled with the liquid, to the extent possible given the constraint of the solid grain sizes and packing. Some of the solid will dissolve into the liquid, which allows for better packing.

Solution-precipitation is the second step in the process, and is when the particles of the powder stop moving mechanically and atomic movement is through dissolution and precipitation [36]. At points in the solid with a higher chemical potential, due to either capillary stress from the liquid or a range in particle sizes (smaller particles will have a higher chemical potential), the solid will dissolve into the liquid and deposit onto sites with lower chemical potential. This leads to grain growth as it would in solid state sintering.

The last stage, densification, is when the material comes to the "minimum energy grain shapes" [38], and these grain shapes depend on the dihedral angle [36].

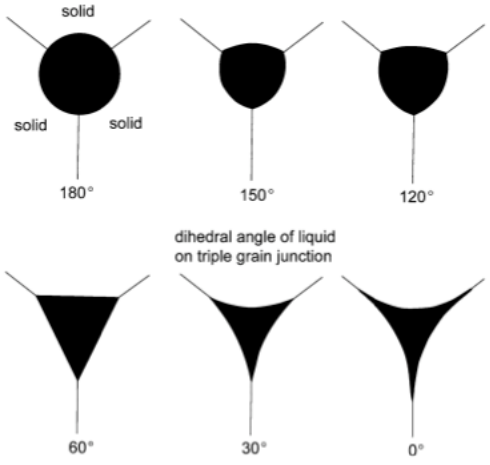

Figure 22: The dihedral angle's impact on microstructure. Figure from [37].

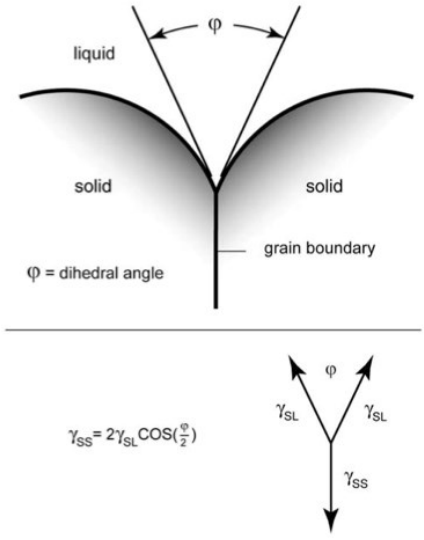

Figure 23: The balance of forces associated with the dihedral angle. Figure from [37]

As seen in Figure 23, the dihedral angle is the angle "of the grain-grain contacts with the liquid phase" [37] and it comes from the energy balance of the

surface energies between solid-solid and the solid-liquid. It is worth saying that the dihedral angle is not always uniform across a sample, there can be a distribution. This is caused by anisotropic surface energies and various misorientation angles [38]. As seen in Figure 23 it is defined by the equation $\gamma_{ss} = 2\gamma_{sl}\cos(\frac{\Phi}{2})$ (13) where γ_{ss} is the surface energy between the two solid surfaces, γ_{sl} is the surface energy between the two solid and the liquid, and Φ is the dihedral angle.

Liquid phase sintering has several advantages, and disadvantages, compared to solid state sintering. One of the biggest advantages is a reduction in sintering time. The liquid phase involved allows for much faster diffusion than solid state sintering, which relies on diffusion through a solid, a much slower process. Liquid phase sintering can often be done at a much lower temperature than solid state sintering of the pure compound alone. Some materials, such as Silicon Nitride, are difficult to sinter in a traditional pressureless solid state sintering route. Because of the material's covalent character it has a low diffusivity [38] making it difficult to sinter. However, with the addition of various additives that produce a liquid phase, the material has been sintered to 99% theoretical density [38].

Liquid phase sintering however can have disadvantages [38]. A larger percentage in liquid phase can lead to a lower hardness and elastic modulus values, because the liquid phase is often softer than the solid phase upon hardening. Liquid phase sintering can also have a deleterious effect on the electrical conductivity of a material, because the intergranular second phases may not be as conductive as the host grains.

A liquid phase sintered thermoelectric material theoretically would have several benefits. As seen earlier, thermoelectric materials can be difficult to make, and often can require high heating temperature and long processing times, or can require techniques that are better for small scale samples, not for large scale production (such as hot pressing or spark plasma sintering). Liquid phase sintering could allow the production of thermoelectrics at lower processing temperatures and over a shorter length of time. Furthermore, it could be applied to a process that makes large numbers of thermoelectrics efficiently in an industrial setting.

The liquid phase itself could have several benefits for the thermoelectric properties of the material. Grain boundaries and secondary phases have been shown to lower the thermal conductivity of a material through scattering of phonons. Furthermore, if a transient liquid phase develops that can penetrate into the grains, it could be used to dope the material and possibly raise the electrical conductivity. This would be advantageous because the lowering of thermal conductivity could lower the electrical conductivity, but doping the material could retard this and serve to further raise the figure of merit of the material. Furthermore, though excessive grain coarsening may be a concern, it has been shown that nanoscaled materials can be made through liquid phase sintering. Ji Woo Kim *et. al.* were able to make a nanoscaled TiN/TiB_2/Fe-Cr-Ni material through liquid phase sintering, seen in Figure 24.

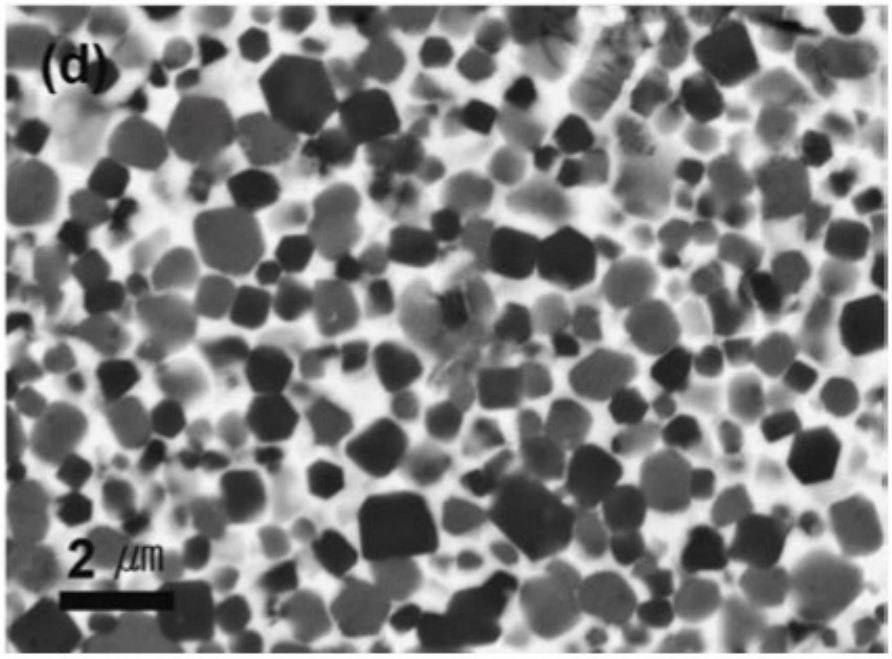

Figure 24: Nanostructured TiN/TiB_2/Fe-Cr-Ni by liquid phase sintering. Figure from [39].

The material was prepared by mechanical alloying, then dry pressing and sintering. For thermoelectrics to reach their full potential they are likely going to need to be nanostructured, and the study from [39] shows that liquid phase sintered samples can be nanostructured, giving hope that this can be replicated for thermoelectric materials.

2.7 SEM/EDS

Scanning electron microscopy is an invaluable technique for determining the microstructure of many polymers, ceramic, and metallic materials. These materials often have microstructural features that are too small to be observed with an optical microscope, necessitating an electron microscope.

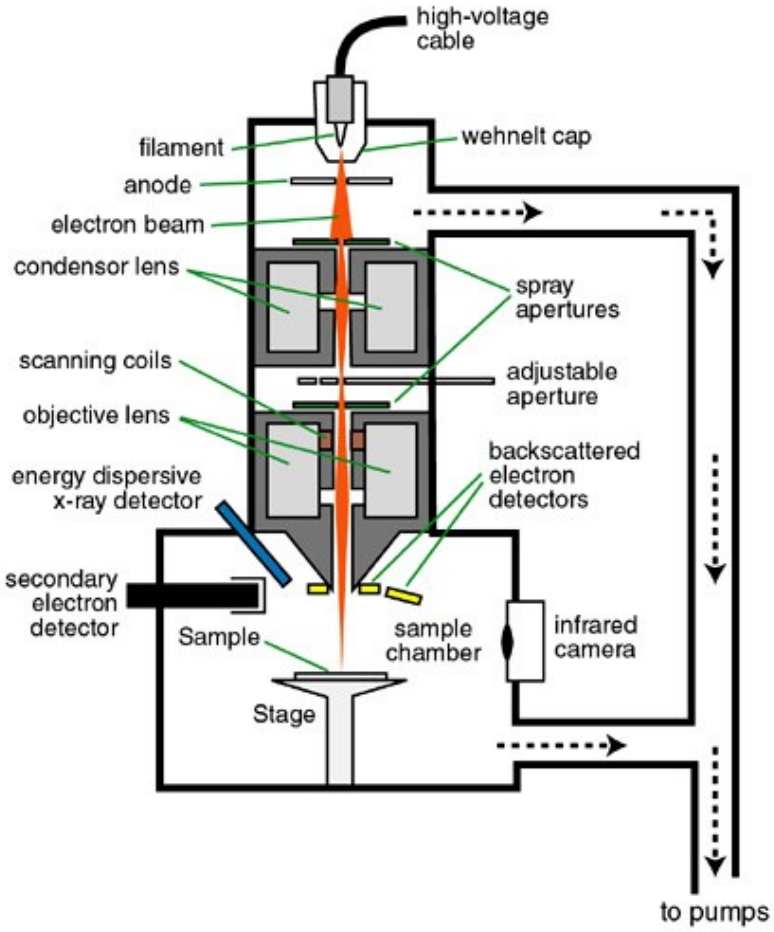

Figure 25: Diagram of a scanning electron microscope. Shows the path of the electron from the source, to the specimen, to the detector. Figure from [40].

The first step is to generate an electron in the electron gun, usually by passing a current through a filament made of lanthanum hexaboride or tungsten, or from a field emission electron gun [41]. The type of source impacts the final resolution of the sample, with lanthanum hexaboride and tungsten providing a resolution of 5 nanometers, while field emission guns provide a resolution of 1 nm [41]. From there several lenses (seen in figure 25) focus the electron beam through magnetic fields [42] to the sample. The beam is often so large that a good quality image could not be produced from it, so it is rendered smaller with the lenses.

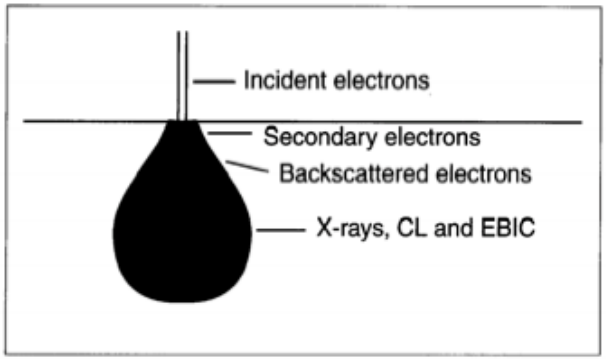

Figure 26: Electron penetration depth. This demonstrates the multiple modes that can be used in an electron microscope and their corresponding sampling depth. Figure from [41].

The electron then enters the sample, and can come out of the sample in several different modes. Secondary electron is the most commonly used, and provides topographical information about the sample. Secondary electrons (seen in figure 27) are knocked out from atomic orbitals by the incoming electrons.

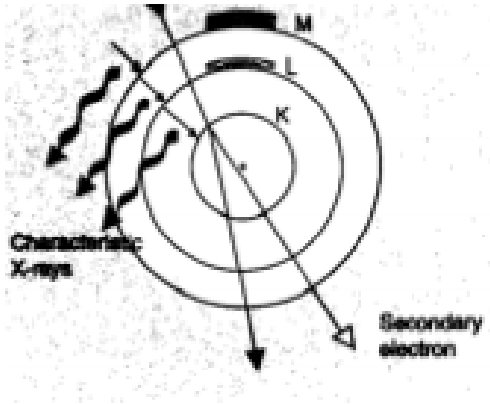

Figure 27: Secondary electron displacement mechanism. Figure from [41].

Some electrons from the microscope do not hit the electrons in the sample, but collide with the nucleus of the sample and are scattered back towards a detector. These are called “backscatter electrons” from which phase information can be gleaned [41]. Since atoms of various elements have different atomic masses, the backscattered electrons appear differently, from which phase information can

be gleaned. This is invaluable for characterizing samples that have been liquid phase sintered, because usually the liquid phase has a different composition than the solid phase, so backscattered electrons can be used to distinguish the phases.

Energy-Dispersive X-ray Spectroscopy (EDS or EDX) can be used to identify elements within a sample. In this technology, an electron beam is used to create X-rays in the sample [42] by the mechanism seen in Figure 28.

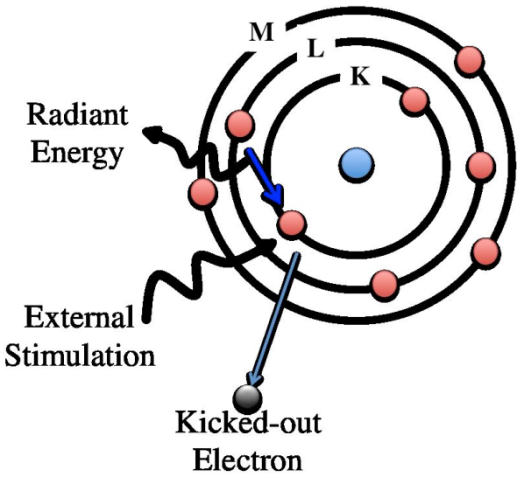

Figure 28: Mechanism for generating x-rays from a sample. EDS takes advantage of the phenomenon to identify elements within a sample. Figure from [43].

If the sample is hit with a sufficiently high-energy electron beam, an electron is ejected from a core level in the sample, while another electron drops from a higher energy level to fill the vacated spot. The difference in energy is ejected as the form of an x-ray, and this energy is characteristic of individual atoms and the specific energy transition (Figure 28 shows a L-K transition [43]). This L-K transition is called a Kα x-ray [44], and each one is characteristic of the element it comes from. This is then detected, and can be plotted against the raster-scanned image to plot where individual elements are within the sample. Between secondary electrons giving topographical information, backscattered electrons giving phase

information, and EDS giving the identification of these phases, a complete microstructural picture can be gleaned from the sample.

2.8 PbTe/Ag_2Te System

Recently, G. Jeffery Snyder and his research group have published several papers on a PbTe/Ag_2Te system that has shown a great deal of potential. It is the system that we have chosen for study, so it is worth discussing.

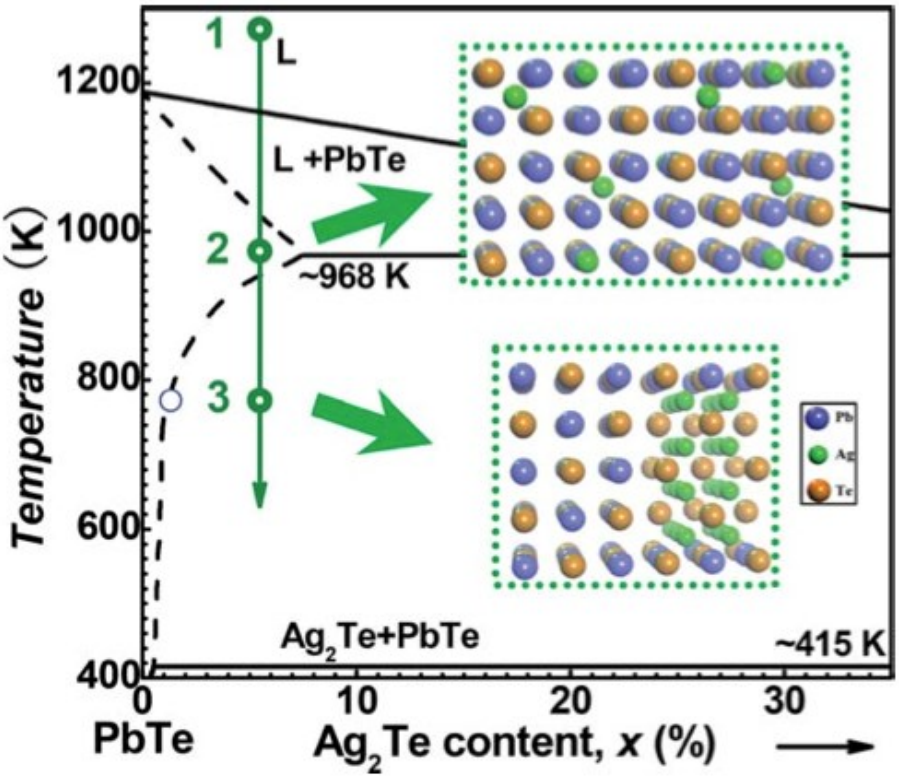

Figure 29: Phase diagram highlighting steps in the synthesis of PbTe/Ag_2Te. This figure, from [13], also highlights the microstructures at several of these points.

This material is synthesized in a three-step process [45], each of which gives a different phase equilibrium as seen in Figure 29. First the material is melted, 1 in

Figure 29, and then cast and allowed to homogenize (2). The material is then brought into the solid region of the phase diagram, where phase separation occurs (3). This approach allows for a high number of precipitates to form, as seen in Figure 30. These precipitates lower the materials thermal conductivity by deflecting phonons as discussed earlier.

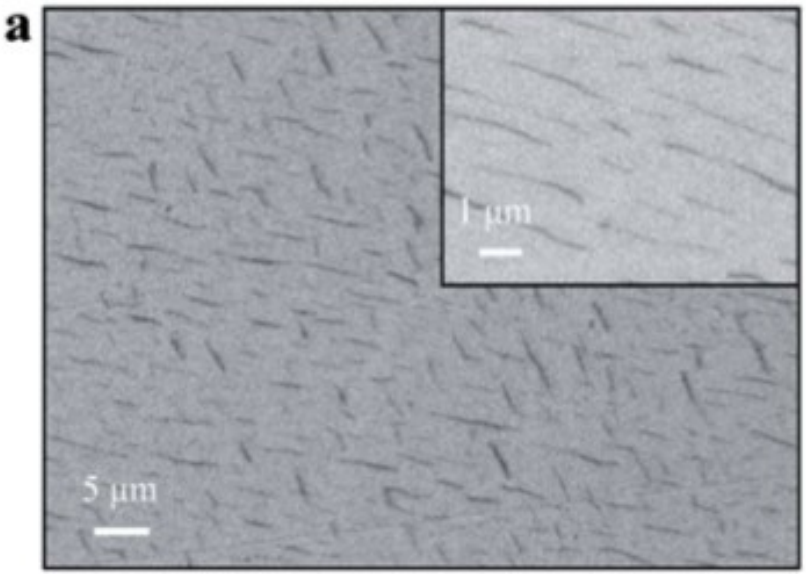

Figure 30: SEM of PbTe/Ag_2Te material. The dark phases are the Ag_2Te precipitates capable of scattering phonons. Figure from [13].

When the material is synthesized without doping, the figure of merit is increased, reaching a maximum above 1 [46]. However, it has been found that by doping the material even better figures of merit can be achieved. In [13] the material was doped with Na, which led to a figure of merit of 1.5 at approximately 650K. This is because the inclusion of sodium increases the density of states at the Fermi level

[47], raising the Seebeck Coefficient, which in combination with the nanostructuring increases the figure of merit of the system to 1.5.

A similar system with similar results can be developed when the PbTe/Ag_2Te system is doped with lanthanum [3]. The lanthanum increases the carrier concentration of the material, increasing the electrical conductivity by more than an order of magnitude (compared to undoped samples). The thermal conductivity is improved, due to "alloy scattering in the PbTe solution matrix and boundary scattering from the nano-precipitates" [3]. This is an excellent accomplishment, because it allows for separation of electrical and thermal conductivities, which are usually coupled.

This doping makes for an n-type material, which is useful because a thermoelectric couple requires both p-type and n-type legs. This further develops this useful system, as the result from [13] was p-type. Were this system brought to market, it would allow the manufacturer to easily make thermoelectric modules, since only one "variable" (i.e. the dopant) would need to be changed. This gives hope to the idea that this system could be industrially robust.

This system has been continually studied and better understood. The Snyder group published a paper [12] that explored the exploring the phase diagram of the system, finding the solvus line as well as important solubility information.

The group was also able to attempt to optimize the carrier concentration for the material [46], allowing the material, which is already very customizable, to be engineered so it is better suited to the application. Figure 31 shows this effect, where the optimum carrier concentration is shown for several temperatures.

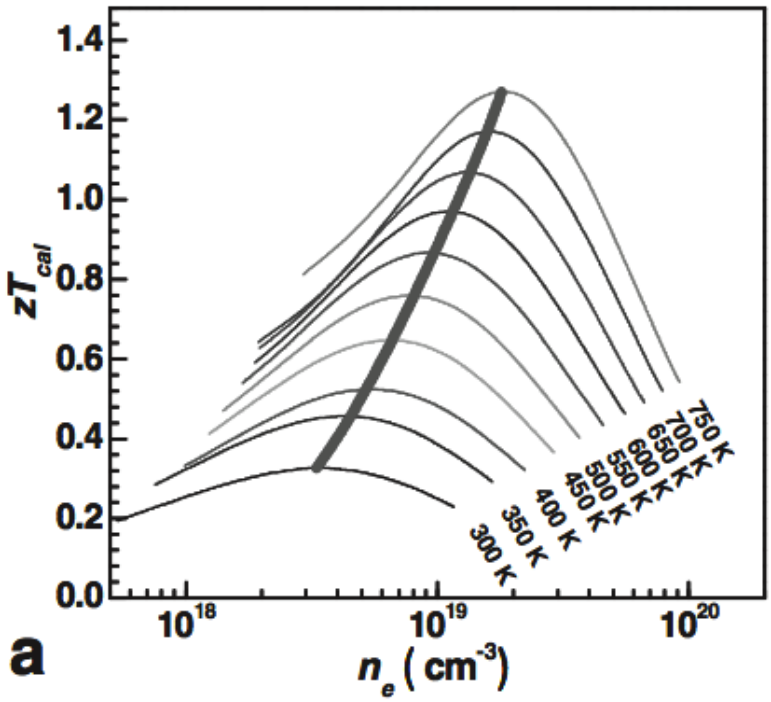

Figure 31: A graph comparing extrinsic carrier concentration to the corresponding figure of merit at several temperatures. This graph could be used to optimize the carrier concentration at application specific temperatures to achieve the maximum figure of merit. Figure from 46.

These calculations for optimum carrier concentration could be used to "grade" the material [46], and improve its performance in a thermoelectric module. As previously mentioned, compound legs of a module can be made to take advantage of materials that are better at particular temperatures. However, this is only two materials. If the leg of the module could be engineered to have more than 2 materials or one material with an increasing gradient of charge carriers, this figure could be improved even more. Clever device design would be necessary, because diffusing the dopant across several millimeters of compound to get the graded

material would be impractical. However, if this could be overcome, it could lead to devices of greater efficiency.

This system was chosen for our present work because it matches several of the criteria necessary for our research. We were looking for a lead telluride system, with good thermal and electrical characteristics. More than that, it had to be a system that could be sintered with a liquid phase sintering approach. Many good lead telluride based systems exist now, such as PbTe/PbS and PbTe/PbSe, but for the most part they possess phase diagrams that would not allow for liquid phase sintering. They are either non-eutectic or have a liquid phase that would not work since the section of the phase diagram containing the liquid phase is too narrow. The PbTe/Ag_2Te phase diagram has a large solid plus liquid phase on the lead telluride side, allowing for many liquid phase configurations to be used. Further the work of Pei, *et al* had shown the beneficial internal precipitation process that lowered the thermal conductivity. So working with a Ag-rich liquid phase could lead to composition conditions that would also promote internal precipitation during processing.

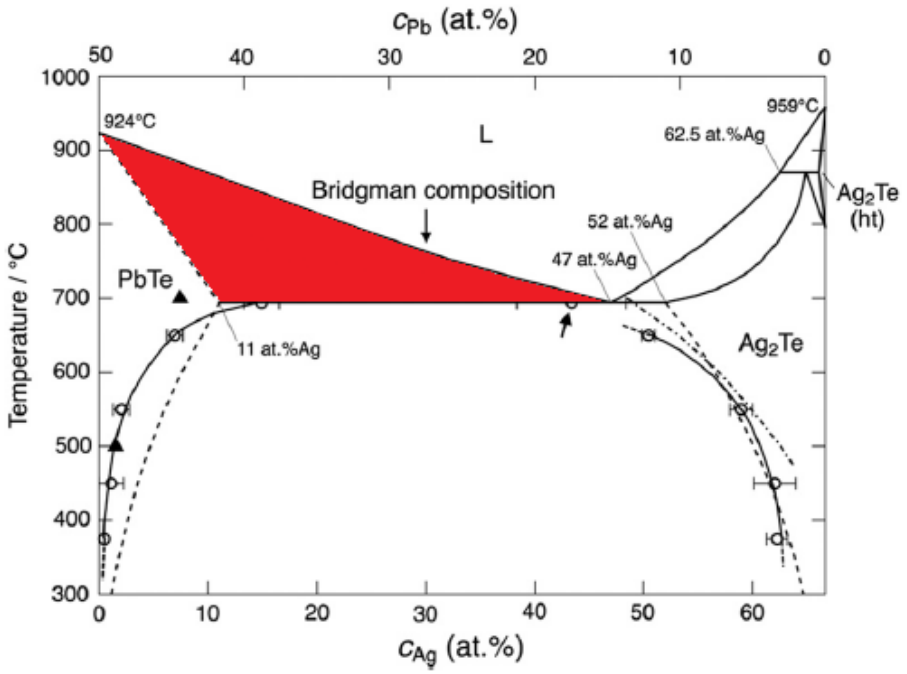

Figure 32. Phase diagram for the PbTe/Ag_2Te system. This system features a large S + L region, colored red, which was a factor in choosing this system. Figure from [12].

3. Experimental

Reduction of Particle Size:

Lead telluride was obtained from Sigma-Aldrich and silver telluride from Fisher Scientific in the form of chunks. These were then separately ground in a grinder from Janke and Kunkel. The resulting powder was then collected and mixed into powder containing ten atomic percent silver (or not mixed for the undoped sample). These powders were then placed in plastic Nalgene bottles with hexane and zirconia milling media, and then ball milled. The undoped sample was milled for 20 hours, and the doped sample was milled for 5 hours. The resulting powder

was then sieved to separate it from the milling media, and allowed to dry. As much of this as possible was performed in a fume hood to prevent lead contamination.

Pressing

The mixed powder was taken and placed into a circular pressing die, diameter 10mm. This was then transferred to a Carver press, and was pressed at 521 MPa.

Heat Treatment

The pressed samples were placed in alumina crucibles, and placed into tube furnaces with fused silica tubes and water cooled stainless steel end-caps. The samples were then heated, to 650^{o}C for the undoped sample and to 750^{o}C for all other samples under flowing argon to prevent oxidation of the samples. The furnace ramp rate was 150^{o}C per hour, and it was cooled at 150^{o}C per hour. The "quenched" sample and the "grid" sample were not cooled at these rates, instead the furnace was shut off and the gas flow rate was increased to cool the sample at a much faster rate.

Preparation for SEM

Samples were prepared for the SEM in one of two ways. Some were either wrapped in a paper towel, then fractured using a razor blade and a hammer. Other samples were mounted on a polishing die and then polished, using progressively smaller diamond pastes down to a ¼ micron diamond paste. The polishing was by

hand, placing the paste on a piece of glass with a small amount of lubricant and polishing against that.

Microscopy:

Fractured and polished samples were examined using a ZETA scanning electron microscope. Multiple modes of scanning were used, including a secondary electron mode to look at topography, a backscatter mode to look at different phases, as well as energy dispersive spectroscopy to identify the various phases within the material.

4. Results:

As mentioned in the Experimental section, all samples were subjected to the same initial treatment, grinding, ball milling, sieving, cold pressing, and sintering under flowing argon. Several samples were made. The first sample was an undoped sample, to see what the microstructure of a "normal" sample would be when the experimental procedures were applied. Doped samples were run with increasing sintering times to see how the microstructure evolved with heating. Some samples were subjected to a slow cool after the heat treatment, while others were cooled at an increased rate to try and "freeze" the microstructure and achieve a greater understanding of how the liquid phase behaved in the sample. All samples were examined with a scanning electron microscope to see how the addition of silver telluride and how differing heat treatments change the microstructure.

Furthermore, an experiment was attempted to see how the liquid moved in a more controlled grain sizes.

4.1 10-Hour Undoped Sample

The first sample that was produced for the study was an undoped sample of PbTe to establish a microstructural baseline for the material. It was important to understand how the material acts during sintering, to see areas that could be improved. Bouad [48] laid out several processing conditions to choose from, from which we chose the "mildest". It involved pressing the material at 420 MPa, and then heating at 650 ^{o}C for 10 hours. The resulting structure was studied by SEM of fractured surfaces.

The fracture surface was relatively uniform, and as seen in Figure 33, it contains uniform porosity. Though the porosity is present, there is also excellent adhesion between the grains.

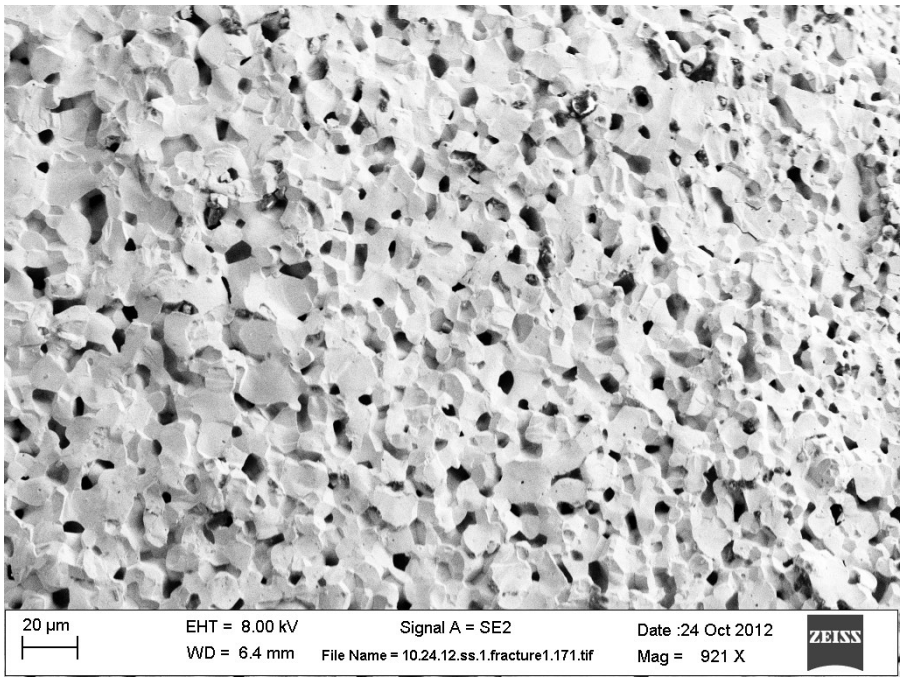

Figure 33: Scanning electron microscope view of 10-hour undoped sample fracture surface, 921 X magnification. This image highlights extensive but uniform porosity.

At higher magnifications, more information can be gleaned about the microstructure. Large dihedral angles are displayed in Figure 34 which is detrimental for achieving a dense ceramic microstructure.

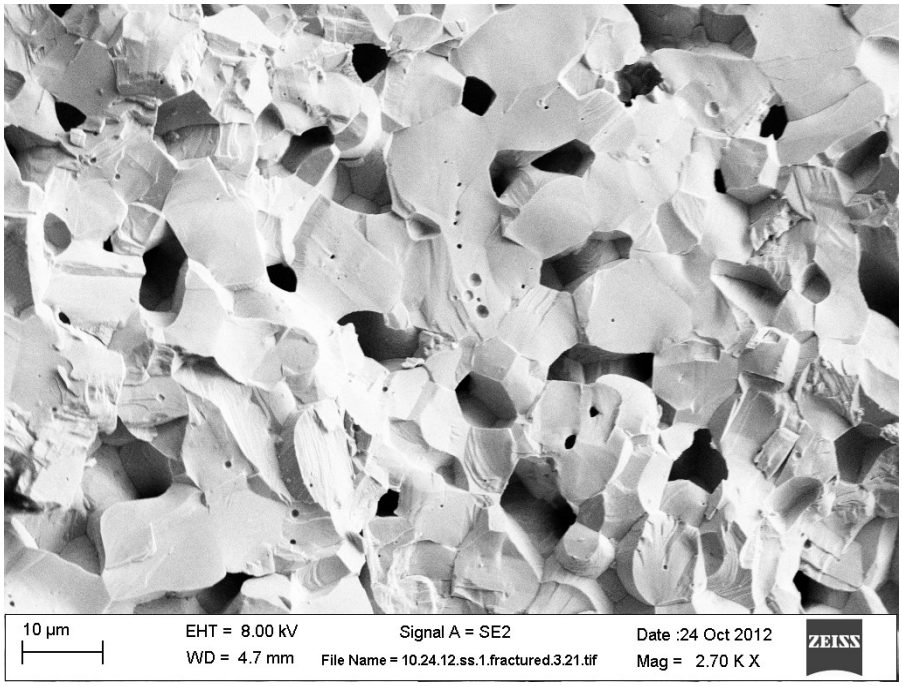

Figure 34: Scanning electron microscope image of 10-hour undoped sample, 2.70 K X magnification. Of particular note are the pores running parallel to the sides of the grains.

From the SEM micrographs, clues can be deduced about how the material fails under stress. Transgranular fractures are seen in Figure 35. This is consistent with brittle fracture, which is logical for an intermetallic ceramic like PbTe.

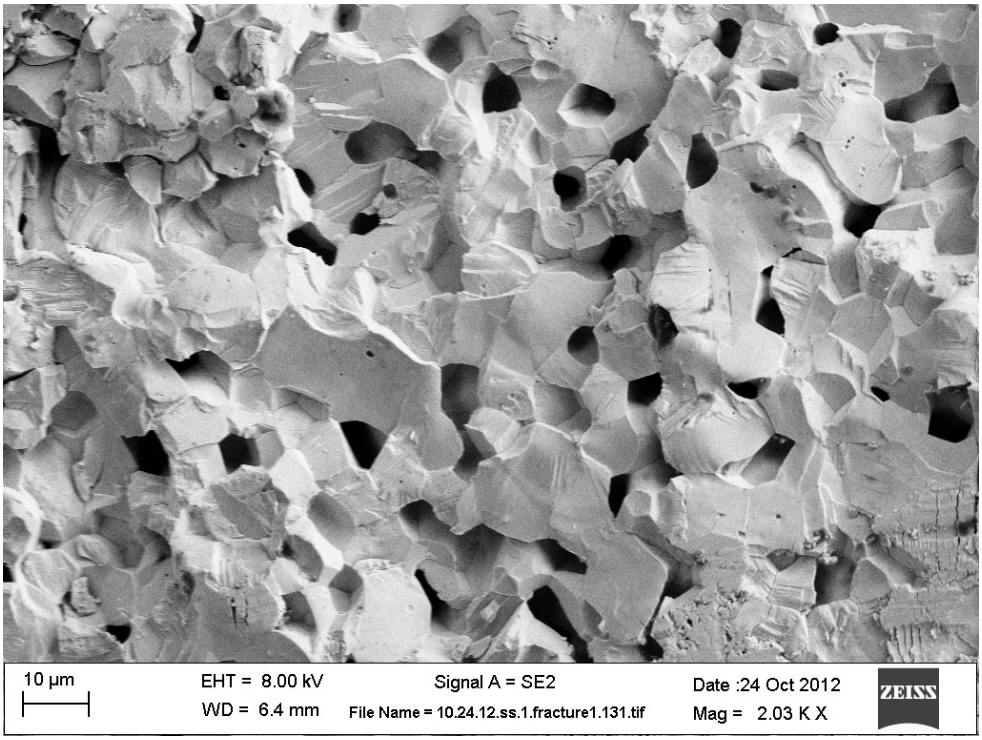

Figure 35: Scanning electron microscope image of 10-hour undoped sample, 2.03 K X magnification. This image illustrates transgranular fracture that occurs in the material.

Throughout the microstructure, and seen in Figure 36 there are "holes" in the middle of grains. These are trapped pores, which are the result of grain growth in a sample. This also indicates that even after 10 hours, this is still in the early stages of sintering,. Trapped pores are usually eliminated as sintering continues. The large amount of porosity supports this theory as well, as does a study by Breschi and Fano it was found that after 90 hours at this temperature the sample was still not "well sintered" [49], making it unlikely that the sample in this study was well into the sintering process.

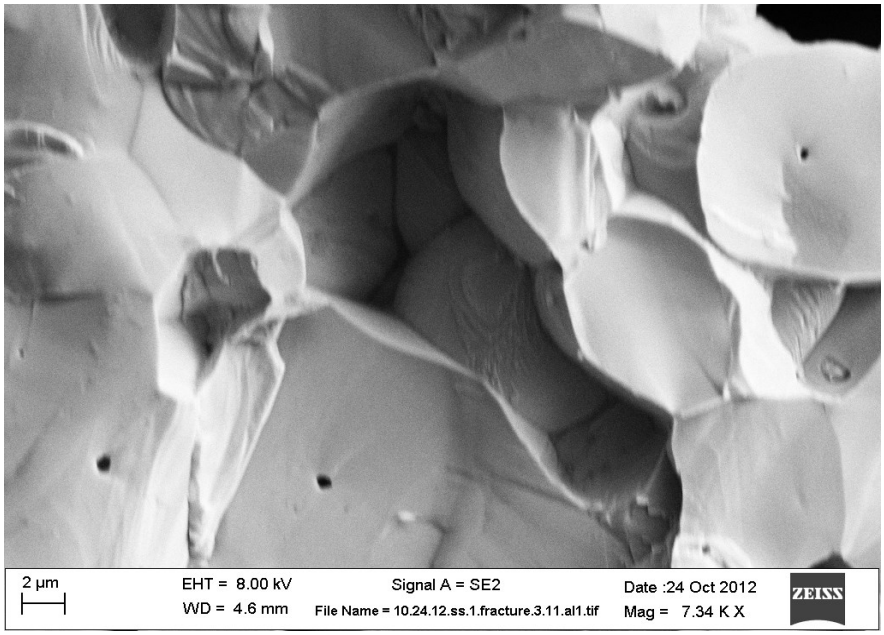

Figure 36: Scanning electron microscope image of 10-hour undoped sample, 7.03 K X magnification. This image is a good view of trapped pores and pores running parallel to the grains

On the inside of larger pores the outside of grains was able to be visualized.

Surface faceting can be seen on the grains in Figure 37.

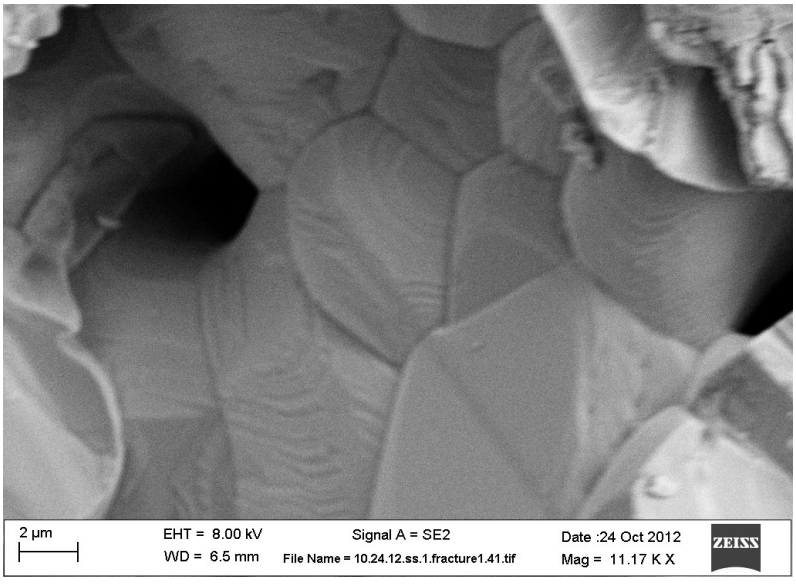

Figure 37: Scanning electron microscope image of 10-hour undoped sample, 11.17 K X magnification. An open area within the sample before fracture, showing high degrees of surface faceting

This faceting is most likely from surface diffusion. According to [36] this is most likely the "Intermediate Stage" of sintering, since "the radius of the neck between the particles has reached a value of 0.4-0.5 of the particle radius," as they appear to in the above micrographs. This analysis seems to be logical, as the intermediate stage is where a sintered material spends most of its time. The compact does not seem to be in the "Final Stage" of sintering. According to [36], during the "final stage begins when the pores pinch off and become isolated at the grain corners." This does not appear to be uniformly the case, as many of the pores are parallel to the long sides of the grains (this is particularly evident in Figure 34).

It was clear from this sample that without doping, long sintering times would be needed (though this was done at a lower temperature than the doped samples experimented on later). Furthermore, while some desirable characteristics were found, particularly the uniformly good adhesion, there were several undesirable characteristics in this sample, such as the high porosity and the fact that it was still in the intermediate stages of sintering.

4.2. 1-Hour Unquenched Sample

A sample was produced with the powder processing conditions laid out in the experimental section, and sintered for one hour at 750^{o}C under flowing Argon, and allowed to cool at the usual rate, while another, which will be talked about next (Section 4.3), was also sintered for an hour and then cooled at a much faster rate. It was then fractured and examined with SEM.

The sample is distinctly different than the undoped sample from above. As seen in Figure 38, there is porosity throughout, but it is not as uniform as the undoped sample's porosity. It does display a similar amount of densification as the undoped sample did; it is sintered for 9 hours less, but at a slightly higher temperature.

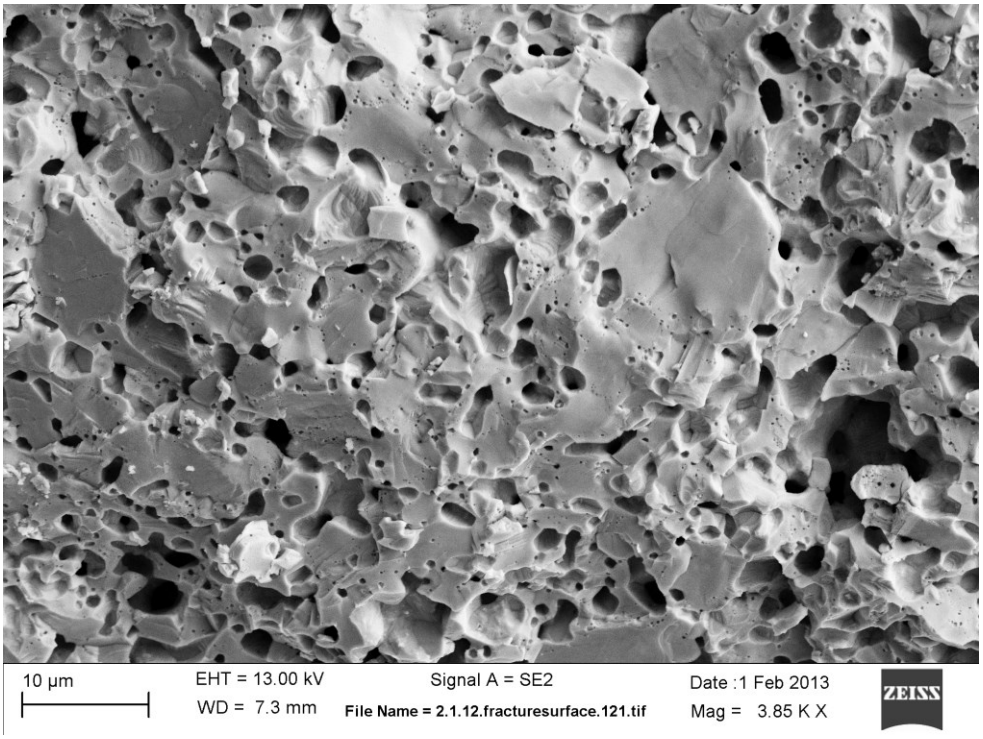

Figure 38: Scanning electron microscope image of 1-hour unquenched sample, 3.85 K X magnification. The microstructure exhibits a similar amount of densification and porosity to the undoped sample.

As seen somewhat in Figure 38, but more in Figure 39, the sample contains a mix of large and small grains, whereas in the undoped sample the grains are all of a similar size. Some grains in Figure 39 are very small and seem to have just started necking. In Figure 39 pores do not seem to have formed yet, there are merely spaces between the grains. From all of this, it seems that this is in a very early stage of sintering.

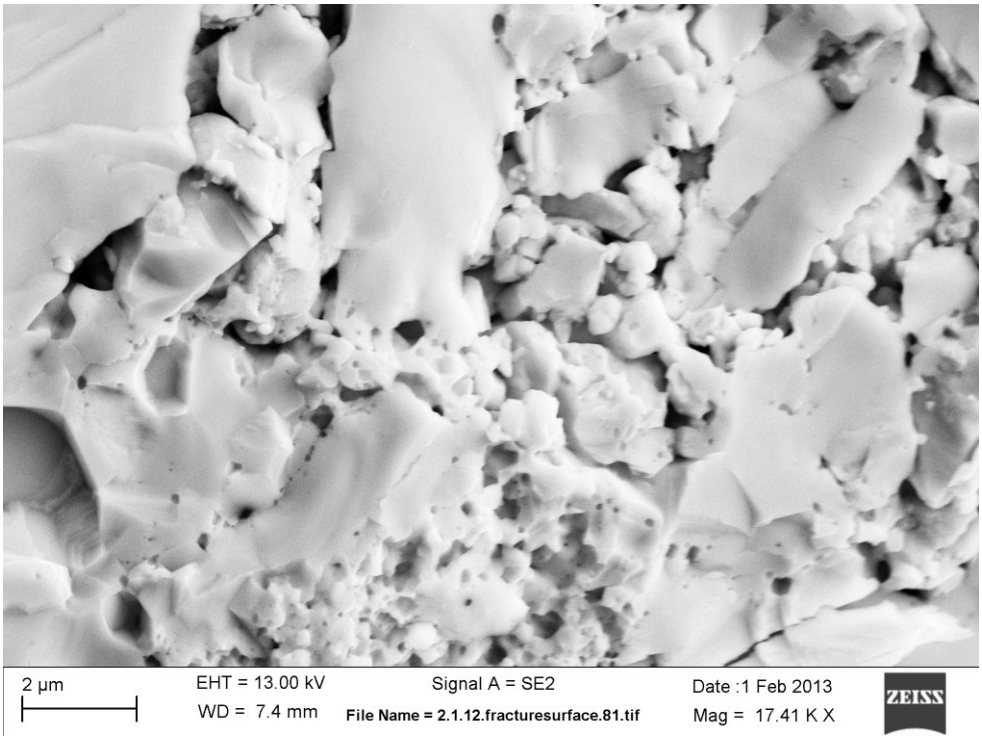

Figure 39: Scanning electron microscope image of 1-hour unquenched sample, 3.85 K X magnification. Micrograph showing some grains that appear to be growing at a much faster rate than the grains next to them.

In Figure 40 a developing grain boundary is seen. It is as if the larger particles are swallowing up the smaller particles, further evidence that this system is still in the early stages of densification. This also could be caused by bimodal grain growth. Areas of the green body that contain silver telluride particles will form liquid at a faster rate, which could lead to enhanced sintering at those locations. This could be what causes some grains to grow faster than others.

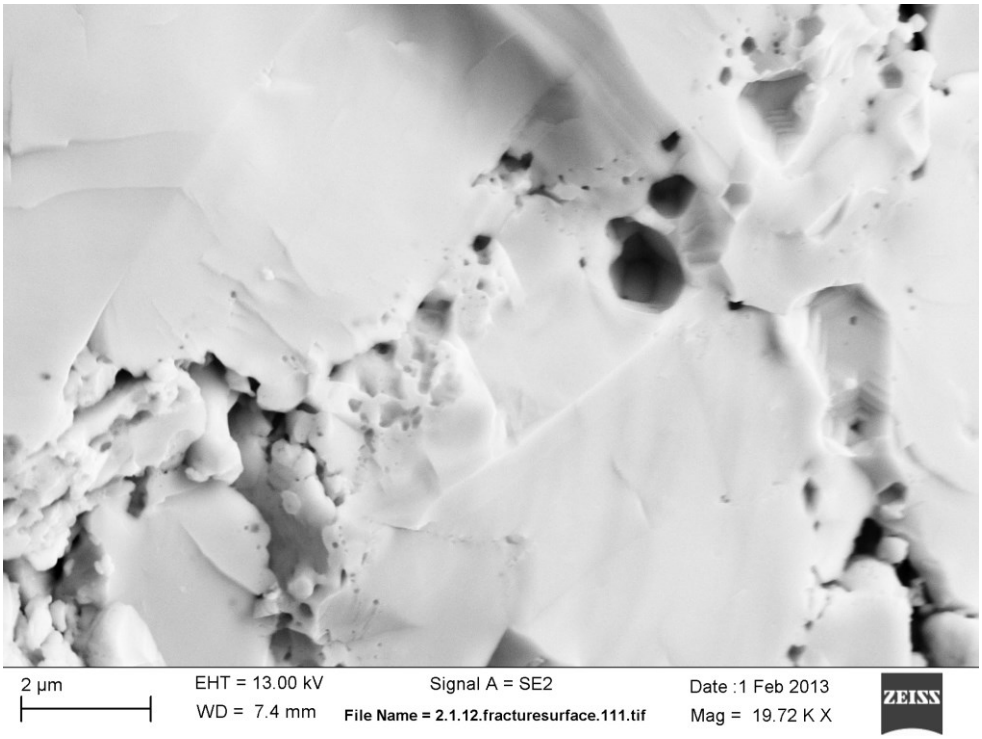

Figure 40: Scanning electron microscope image of 1-hour unquenched sample, 19.72 K X magnification. This image shows a "snapshot" into the complex process of grain growth.

All of these micrographs, and especially in Figure 41 seem to exhibit brittle fracture. The grains themselves fracture into pieces, and not along the grain boundaries. This shows that the system is well into the process of densification, if it had been too early the grains would have separated from each other because they did not have high adhesion.

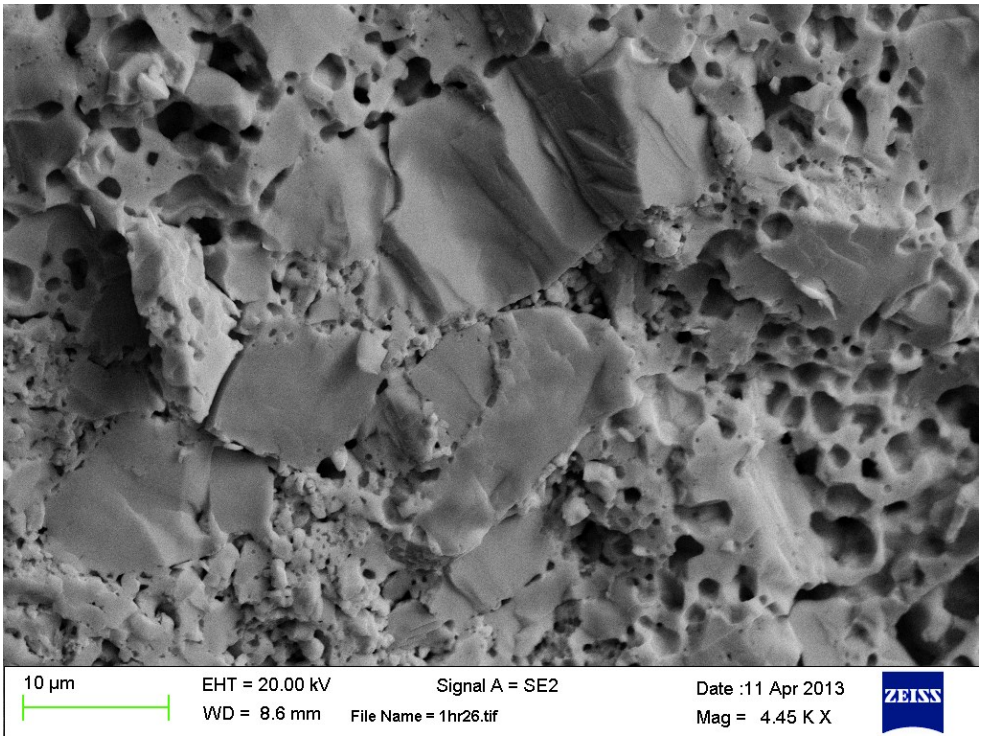

Figure 41: Scanning electron microscope image of 1-hour unquenched sample, 4.45 K X magnification. The sample shows clear brittle fracture, as well as bimodal grain growth. The bimodal grain growth is likely the result of a uneven liquid distribution allowing some grains to grow faster than others.

During the accelerated grain growth associated with liquid phase sintering, pores are often trapped during grain growth. This is very evident in Figure 42, where there are many trapped pores in the interior of grains close to the grain edges. As smaller grains are incorporated into the larger grains, the pores associated with them can be incorporated into the grain as well. During the later stages of sintering, these pores would be eliminated from the grain to reduce the surface area of the sample, as one of the driving forces in sintering is the reduction of the surface energy of the object.

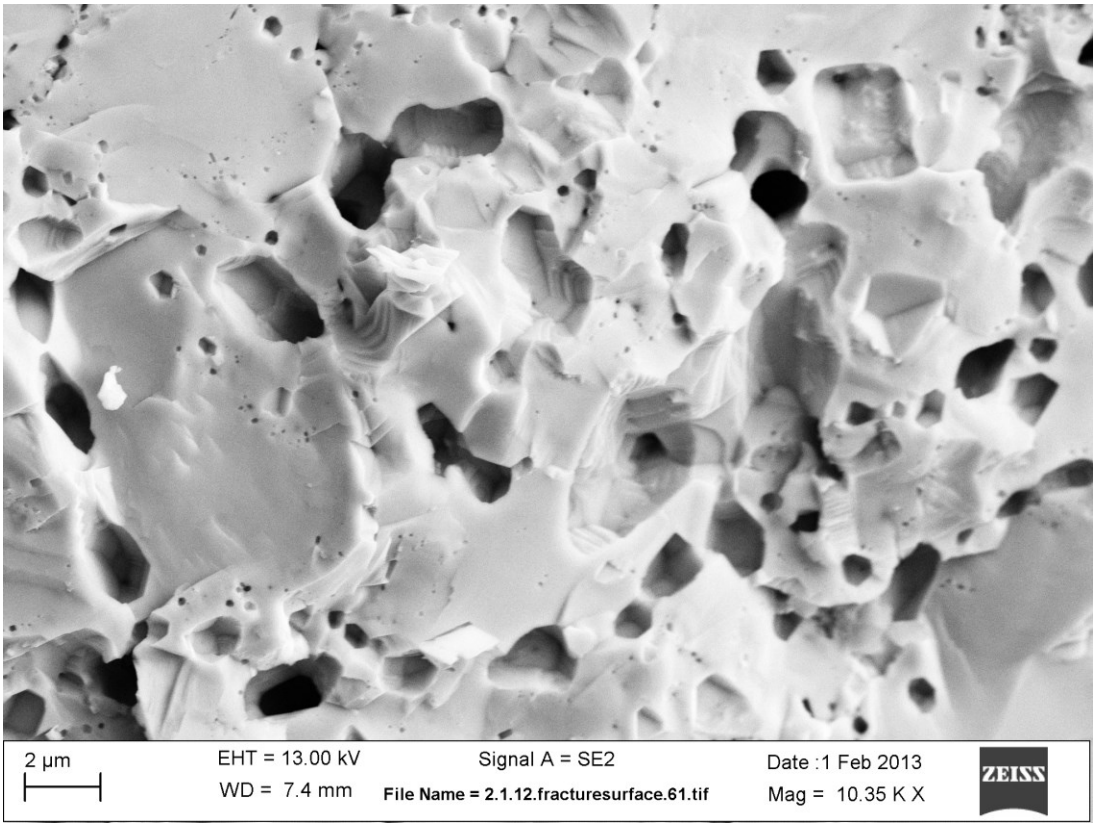

Figure 42: Scanning electron microscope image of 1-hour unquenched sample, 10.35 K X magnification. Many trapped pores are evident on the edges of the grains. While trapped pores on the edges of grains exist in during solid state sintering, the accelerated grain growth associated with liquid phase sintering exaggerates this phenomenon.

In Figure 43 The EDS scans for Figure 41 are shown. It is seen that tellurium is abundant throughout the sample, and the silver is also diffuse throughout the sample. There are some pockets that are silver heavy, but not many. The lead is difficult to see, but the SEM lacked the proper maximum voltage to get a good gain for lead.

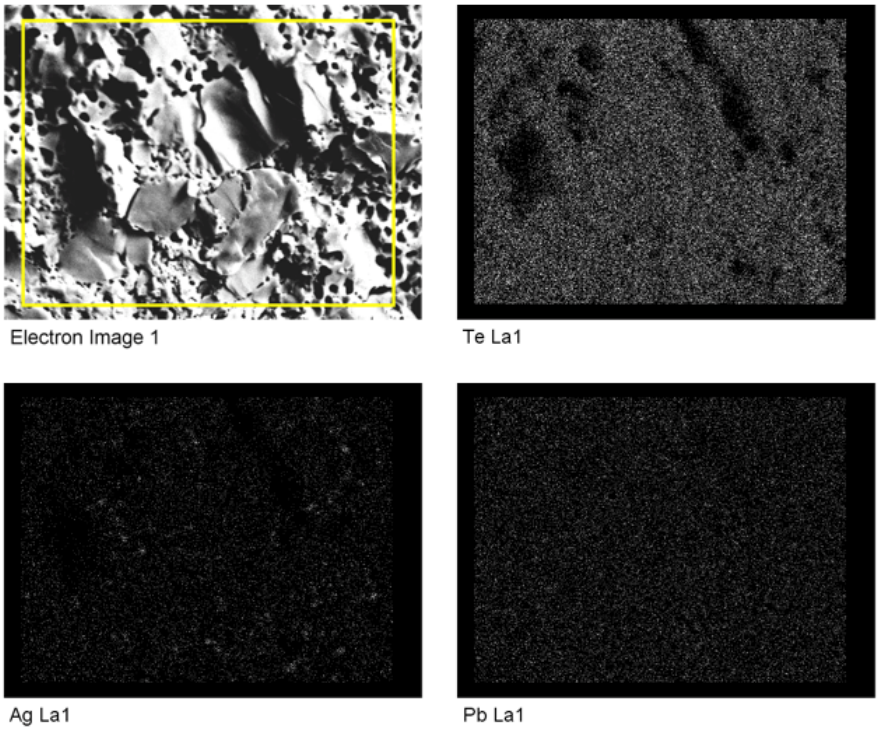

Figure 43: Electron dispersive spectroscopy images of 1 hour unquenched sample. Clockwise from top left: Secondary electron image of the sample, EDS image highlighting tellurium, EDS image highlighting silver, EDS image highlighting lead

This sample showed large amounts of porosity, brittle fracture, a mixture of grain sizes, along with evidence of necking and low grain adhesion all suggest that this is in the early stages of sintering. The promising aspects of the sample are that it has a similar amount of densification to that of the 10-hour undoped sample. Though it was sintered at a slightly higher temperature, the sintering time was much shorter and it allowed for a similar degree of densification.

4.3. 1-Hour "Quenched" Sample

In an attempt to learn more about how the liquid phase cools, a sample was made with a much faster cooling time. As mentioned in the experimental section,

this sample was cooled at a much faster rate than the others, and was then fractured and examined with SEM and EDS.

As seen in Figure 44, the quenched sample looks different from the unquenched one. The quenched sample had a much smaller grain size than the unquenched sample did, as seen in Figure 44.

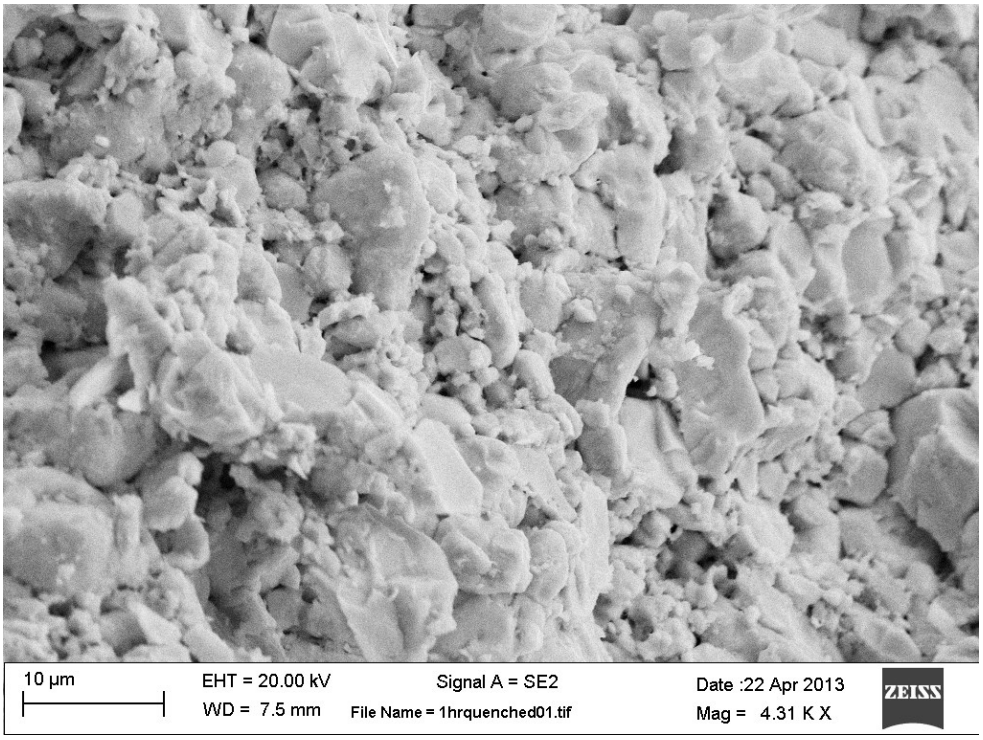

Figure 44: Scanning electron microscope image of 1-hour "quenched" sample, 4.31 K X magnification. This image shows a wide distribution in grain sizes.

As will be seen later in the 2-hour sample, the sample behaves differently by the macroscopic "pores" (Figure 45). The areas directly bordering these pores seem to have experienced more densification than other regions within the sample. Shaw [50] describes a model where a liquid phase during sintering fills smaller pores, as opposed to large ones because there is a capillary pull that draws the liquid from the larger pores to the smaller ones. Here, the liquid seems to have found these smaller

pores, causing the increased densification. There was enough liquid here, that some contrast is seen, even though the micrograph was taken in secondary electron mode. In the three-hour sample (4.5), these darker phases were shown to be silver telluride, which makes up the majority of the liquid phase.

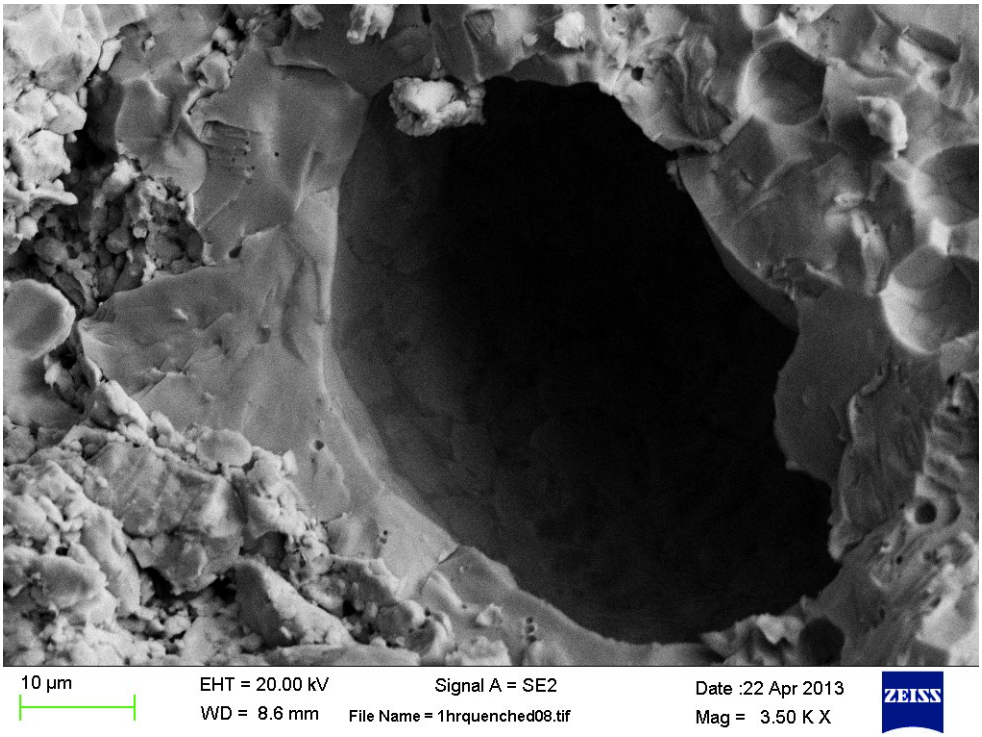

Figure 45: Scanning electron microscope image of 1-hour "quenched" sample, 3.50 K X magnification. This image is a view into a "macro" pore seen in the sample. As mentioned, the darker spots within the pore are indicative of a silver telluride rich region.

The sample also seems to fracture differently than the unquenched sample. The quenched sample exhibited entirely brittle intergranular fracture, while this sample seems to exhibit a mix of transgranular and intergranular fracture Figure 46. It is unknown what could cause this mode of fracture, since a semiconductor such as lead telluride should be experiencing brittle fracture, though this is not what the fracture mode appears to be.

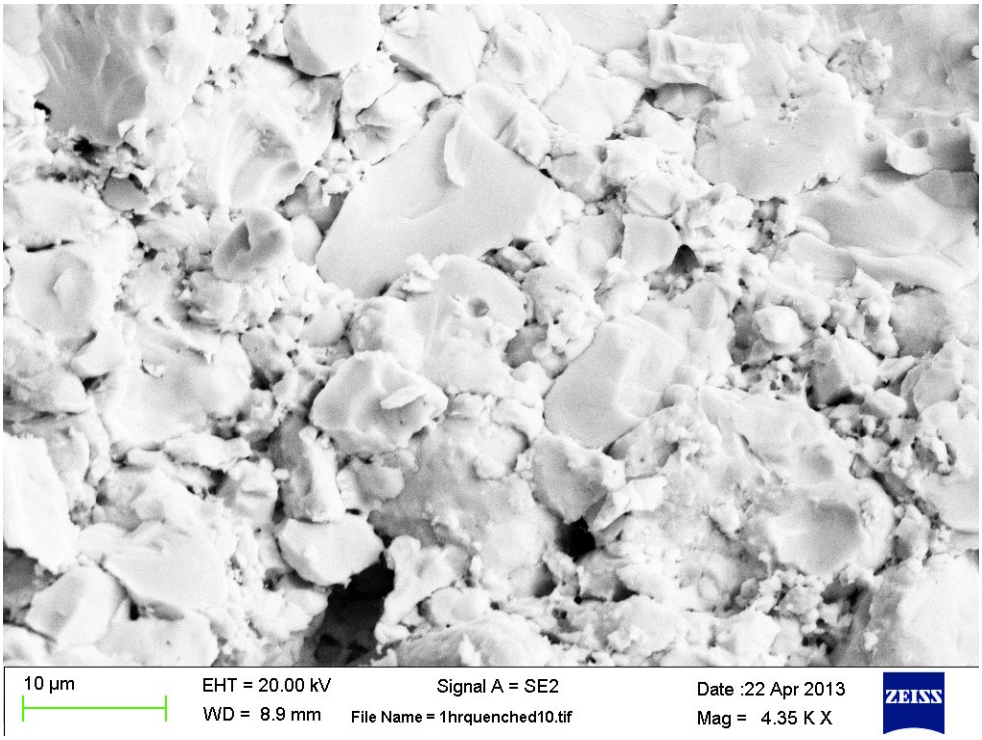

Figure 46: Scanning electron microscope image of 1-hour "quenched" sample, 4.35 K X magnification. The micrograph shows what appears to be a mix of transgranular and intergranular fracture.

When an EDS analysis was performed on the area from Figure 46, shown in Figure 47, the results were shown to be different from the unquenched sample. In the unquenched sample, the silver was relatively evenly dispersed throughout the sample. While silver seems to be present throughout the sample, it is concentrated in many small "pockets" (as shown in Figure 47). It is also seen that many of the larger grains are mostly absent of silver. These are most likely grains that have experienced large amounts of grain growth due to the assistance of the liquid phase, and the silver will only stay in these regions to the solubility limit.

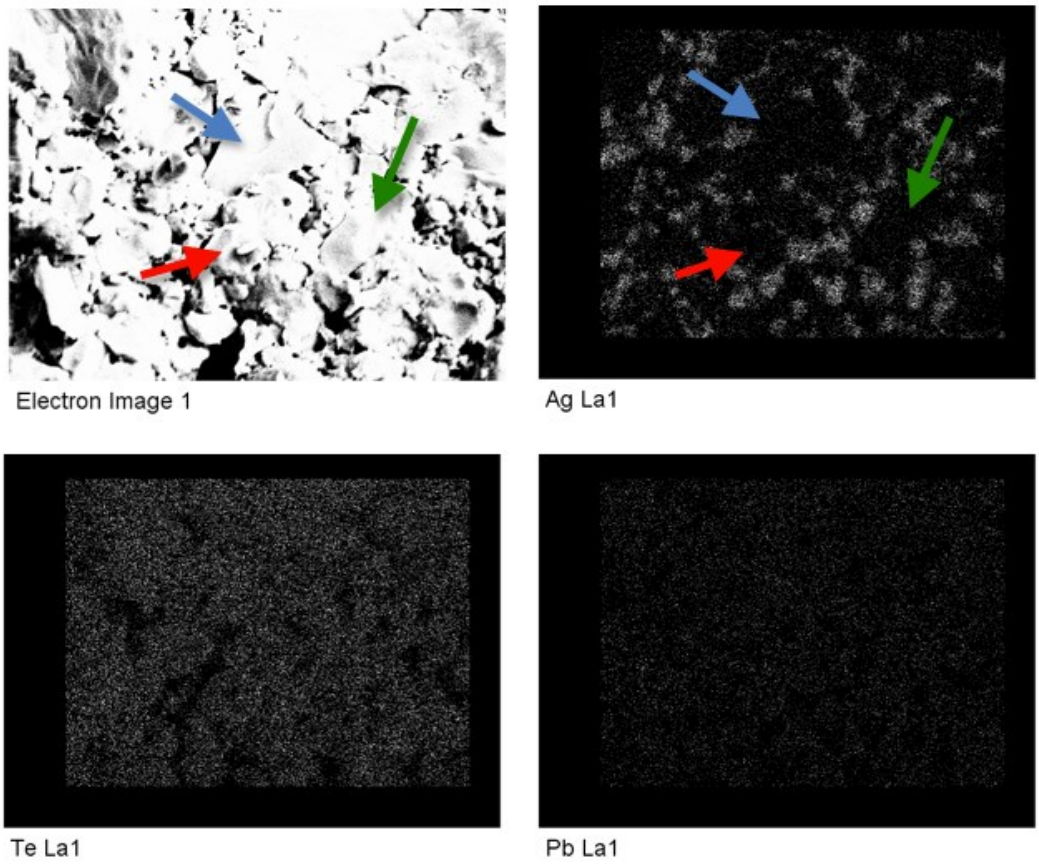

Figure 47: Electron dispersive spectroscopy images of 1-hour "quenched" sample. Clockwise from top left: Secondary electron image of sample, EDS image of the silver in the sample, EDS image of the tellurium in the sample, EDS image of the lead in the sample. The arrows on the on the secondary electron image and the EDS image of the silver highlight some of the large grains in the sample with an absence of silver telluride.

Conclusions can be drawn from this data. In both cases, the samples are heated to 750^{o}C at 150^{o}C an hour. The unquenched sample is cooled at 150^{o}C, while the quenched sample is cooled at a much faster rate. This slower cooling rate would allow diffusion and sintering to continue to occur for the unquenched sample, as a liquid phase would still exist above 690^{o}C. In the unquenched sample, the liquid phase would have approximately an extra half hour to work, and this difference is

seen in the EDS images of the two samples. In the unquenched sample, the silver is shown to be well distributed (Figure 43). The quenched sample lacked this time for the silver to diffuse throughout the sample, and the silver is seen to be in many localized "pockets" (Figure 47). This could be useful in the future if this technology was ever used as a thermoelectric. Once it was determined whether pockets of silver or diffuse silver gave better thermoelectric performance, a suitable cooling profile could be used to provide the necessary disposition of silver.

4.4. 2-Hour Sample

An alloyed sample was produced under the standard conditions for two hours and then was fractured and examined under the SEM and the EDS. It was done both to see if more information could be gleaned about the sintering mechanism at two hours and in hope that the liquid phase could be tracked further.

As seen in Figure 48, from a wide area this sample would seem to have many areas of low porosity, along with some macroscopic pores.

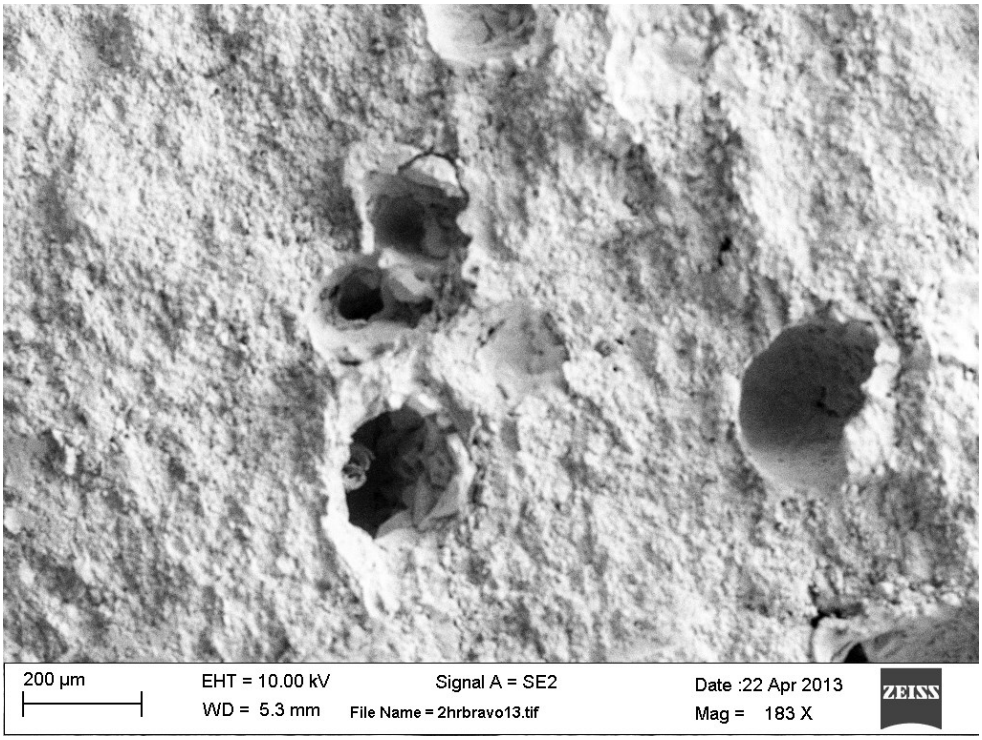

Figure 48: Scanning electron microscope image of 2-hour sample, 183 X magnification. Shows a wide view of the sample.

When the denser areas of the sample are examined under a higher magnification (Figure 49), they are clearly not fully dense. The grains of the sample seem to be packed fairly close together, however they do not seem to be fully joined.

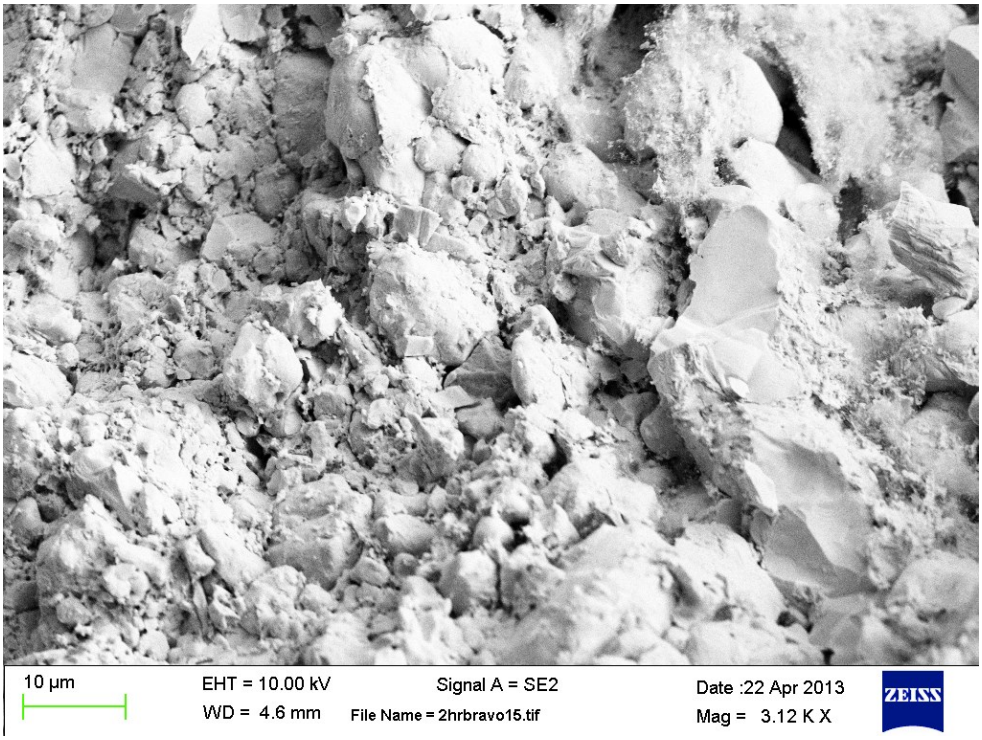

Figure 49: Scanning electron microscope image of 2-hour sample, 3.12 K X magnification. Image shows good particle packing, but poor adhesion.

This would seem to be at either the initial or intermediate stage of sintering [50]. As seen in Figure 50 there are no clearly defined dihedral angles in the sample. Furthermore, the sample has not densified to the point where the pores are "isolated", which generally occurs at the end of the intermediate stage [50], instead they often seem to run parallel to the grains. The particles have small bridges forming between them, which would seem to be indicative of the early stages of necking.

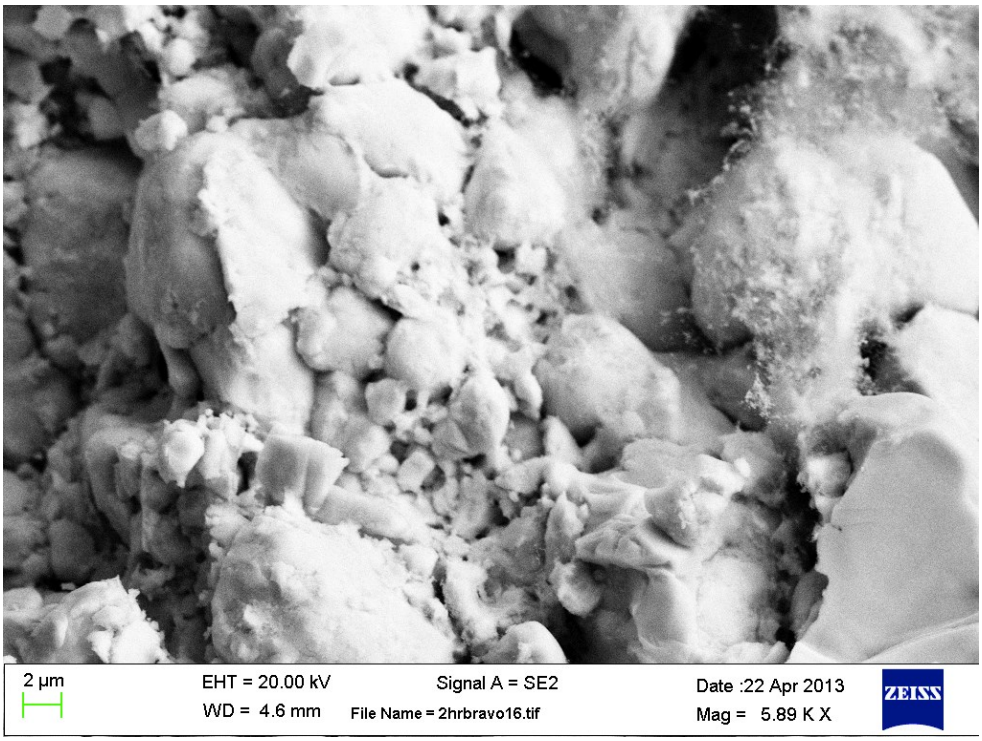

Figure 50: Scanning electron microscope image of 2-hour sample, 5.89 K X magnification. This shows what appears to be the early stages of necking in the material.

Further complicating the analysis is that some particles seem to be farther along in the sintering process than others, as seen in Figure 51. The particles in the middle of the image seem to have consolidated better than the particles on either side. The grain size varies widely over the material, with large grains in the middle of the image and in the upper right corner, and smaller grains spread throughout, which supports the idea that this is still early in the sintering process. Furthermore, Shaw (50) presented a model were the liquid phase during sintering preferentially fills smaller pores over larger ones. These spots would then experience more grain growth because they would have more liquid to assist in the sintering process. The large distribution in grain sizes and amount of densification in Figure 51 would

likely be the result of inhomogeneous pore size, and a resulting inhomogeneous liquid distribution.

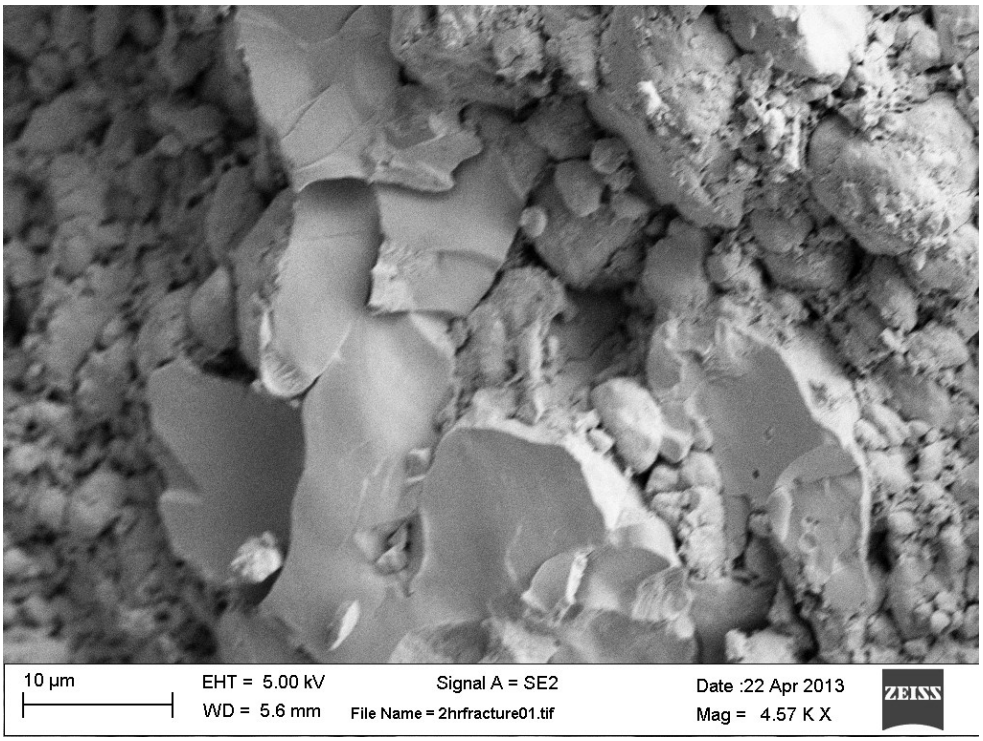

Figure 51: Scanning electron microscope image of 2-hour sample, 4.57 K X magnification. A mix of intergranular and transgranular fracture is evident here.

Evident in in the Figure 51 and especially in Figure 52 is a difference in how the grains fracture. The grains that seem to be farther along in the sintering process fracture in a transgranular mode, while the other grains show intergranular fracture. Since PbTe is a brittle material, it is unlikely that the system is showing some ductile behavior, though it is possible. It is also possible that the parts of the material that are still in the earlier stages of sintering, and as such cohesion between the grains is poor. This causes behavior that appears ductile under these circumstances, but will likely vanish if a fully dense product is achieved.

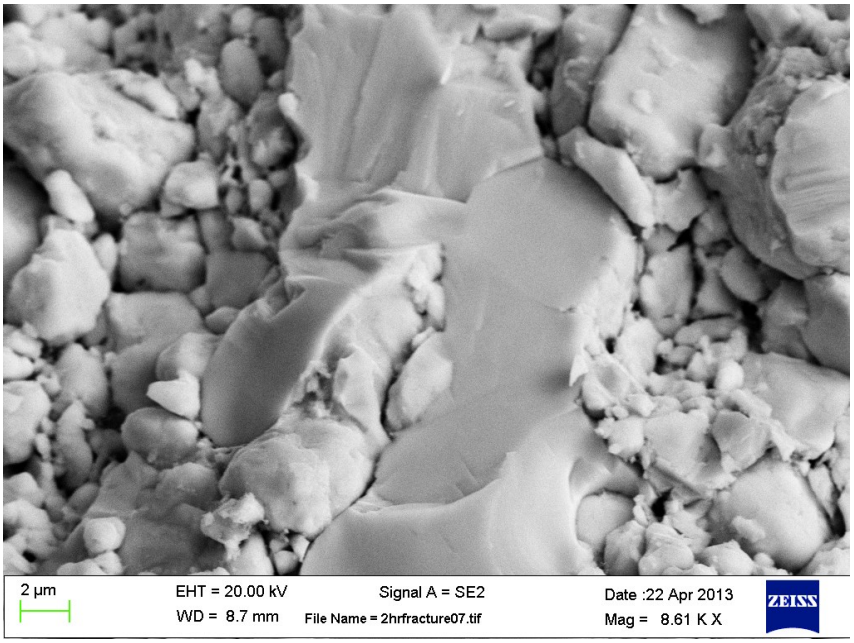

Figure 52: Scanning electron microscope image of 2-hour sample, 8.61 K X magnification. This micrograph highlights a mixture of grain sizes.

In somewhat of an oddity, the areas around the macroscopic pores seen earlier, expanded in Figure 53, appear more densified than areas away from these macroscopic pores.

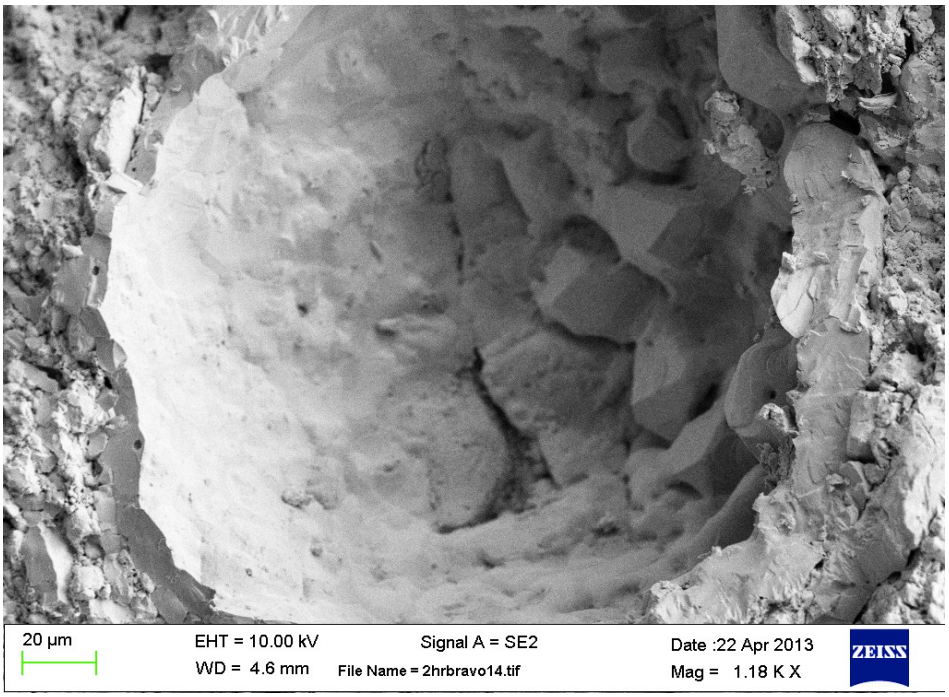

Figure 53: Scanning electron microscope image of 2-hour sample, 1.18 K X magnification. This shows surface of "macro" pores seem to the most densified parts of the sample. The edges of the micrograph show the areas away from the large pore, which do not appear to be as densified.

As seen before, the silver telluride, upon changing to a liquid phase, would "wick" into the smaller pores in the sample, and those parts would then experience greater densification than the surrounding areas. These pores might be caused by unusually high local concentrations of silver telluride after cold pressing, that would then move into the surrounding pores, densifying those areas, but leaving large pores behind.

EDS images were used when trying to find the liquid phase in the sample (Figure 54). The EDS had some difficulty getting a good signal on the lead, but was able to get good signals on both the silver and the tellurium. The scan showed that

silver was distributed throughout the entire sample, but was concentrated at several points.

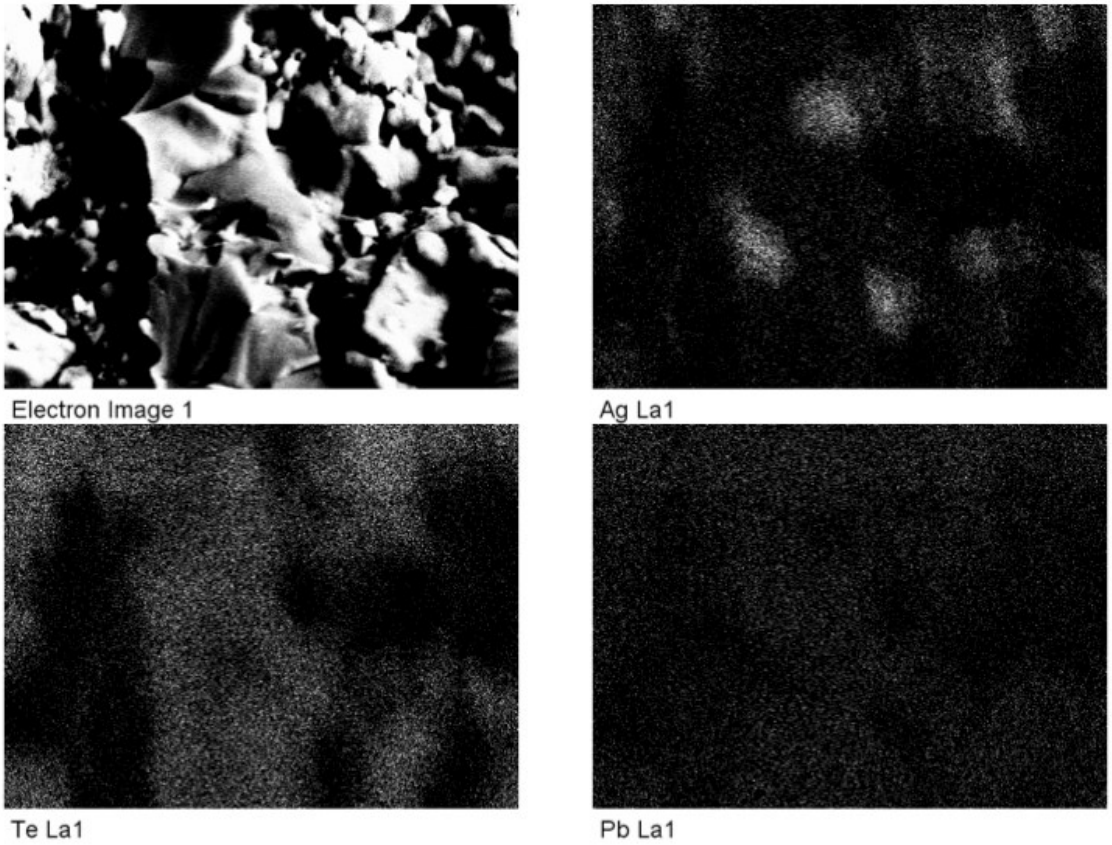

Figure 54: Electron Dispersive Spectroscopy images of the 2-hour sample. Clockwise from top left: Secondary electron image of the sample, EDS image of the silver in the sample, EDS image of the lead in the sample, EDS image of the tellurium in the sample.

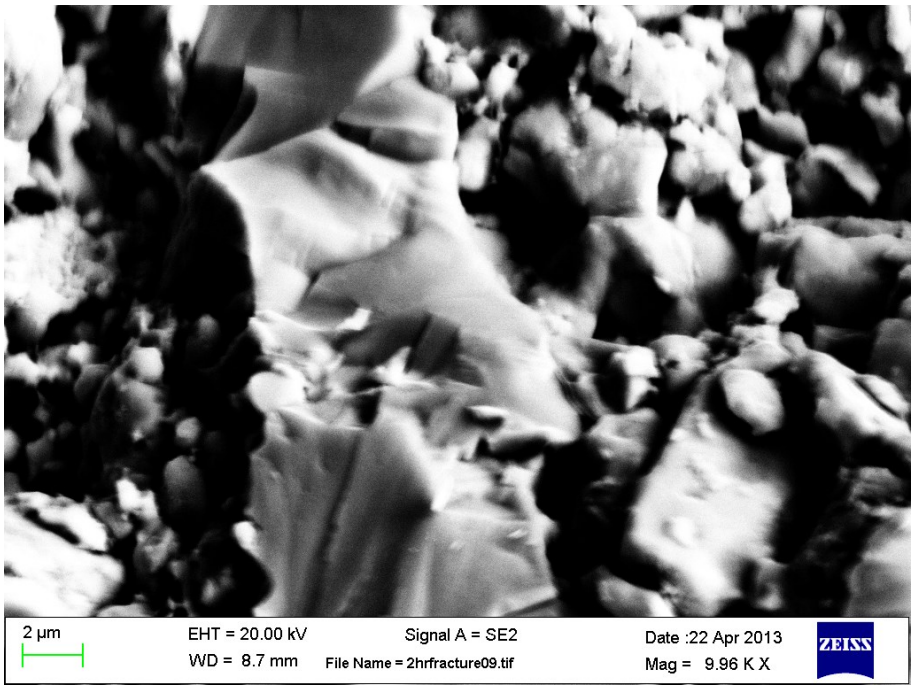

Figure 55: Scanning electron microscope image of 2-hour sample, 9.96 K X magnification. This is the SEM image from figure 54, including a length scale for reference.

This sample would seem to be at the early stages of sintering. The disparity in grain growth, grain size, and the lack of evenly distributed silver telluride (though the 1-hour unquenched sample did have diffuse silver telluride; the unquenched sample did not) would lead one to think that this is still early in the sintering process. The sample does possess some good qualities such as good particle packing, but it is not a finished product yet.

4.5. 3-Hour Sample

When viewed in the SEM, the microstructure of the sintered compact is shown to be complicated. There are areas that contain large pores, as well as areas that have very few pores (Figure 56). When examined with a backscatter detector, different phases of the material are evident (Figure 57). With EDS, it is confirmed that the darker phases are almost entirely Ag_2Te and the light phases are mostly PbTe with some Ag.

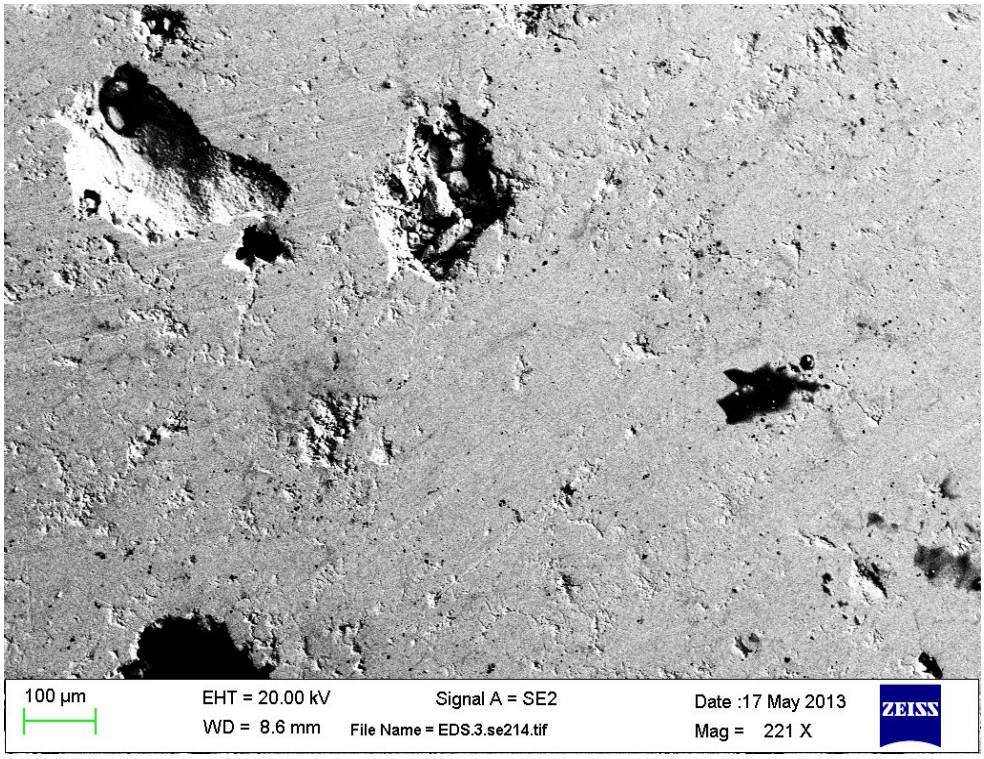

Figure 56: Scanning electron microscope image of 3-hour sample, 221 X magnification. This is a wide view of the sample, showing dense regions as well as voids.

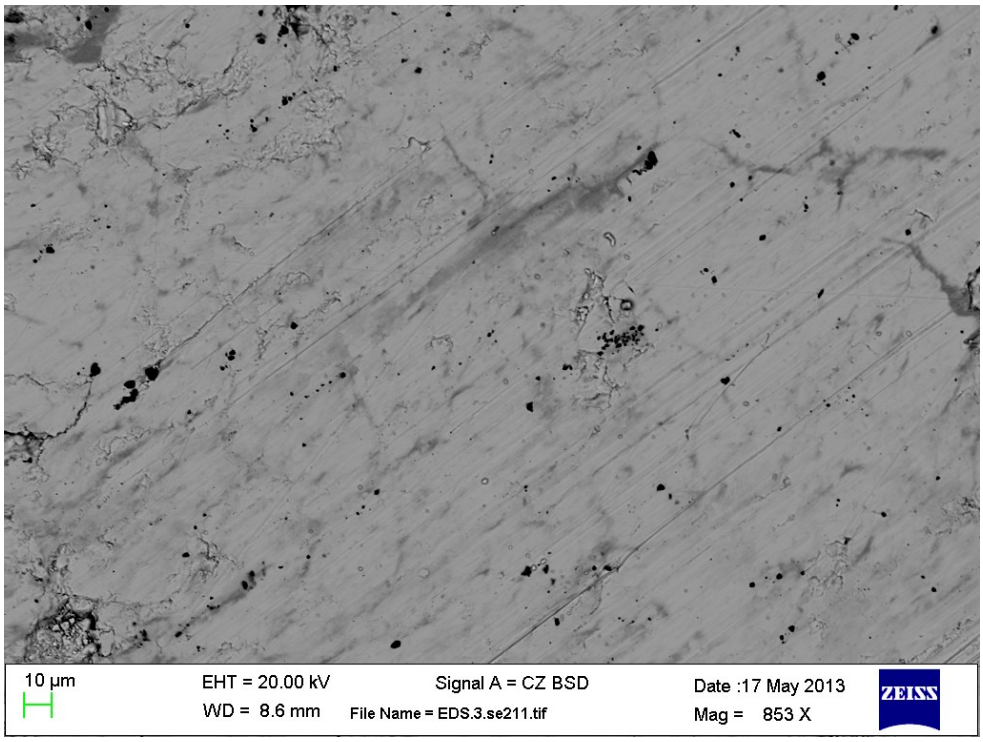

Figure 57: Backscattered scanning electron image of 3-hour sample, 853 X magnification. This shows porosity as well as light and dark phases (lead telluride and silver telluride respectively).

At "exposed" regions, such as inside of the large pores, the microstructure more closely displays the liquid phase sintering history (Figure 58). Clear regions of silver telluride and lead telluride can be distinguished by EDS spectroscopy.

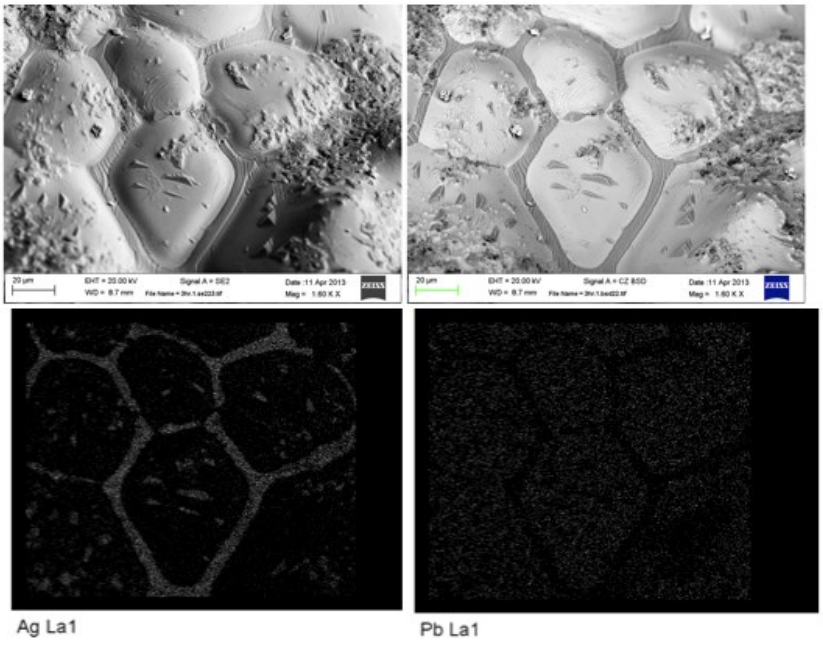

Figure 58: Electron Dispersive Spectroscopy images of the 3-hour sample. SE2 (top left), BSD (top right), EDS of the silver in the material (bottom left), and an EDS of the lead in the material (bottom right). All are from an as-sintered surface within the 3 hour sample.

In Figure 58 the dark regions on the BSD micrograph correspond with the silver rich regions on the EDS. These regions are almost completely devoid of lead, showing that they are silver telluride, not lead telluride doped with silver telluride. The EDS shows some silver inside the lead rich regions, which supports the idea that silver telluride is precipitating out into the lead rich regions, too. It seems that the lead telluride forms grains with some silver telluride dissolved in, and is surrounded by a silver telluride rich liquid.

When regions of the larger pores are examined more closely, as in Figure 59, the microstructure is shown to be even more complex.

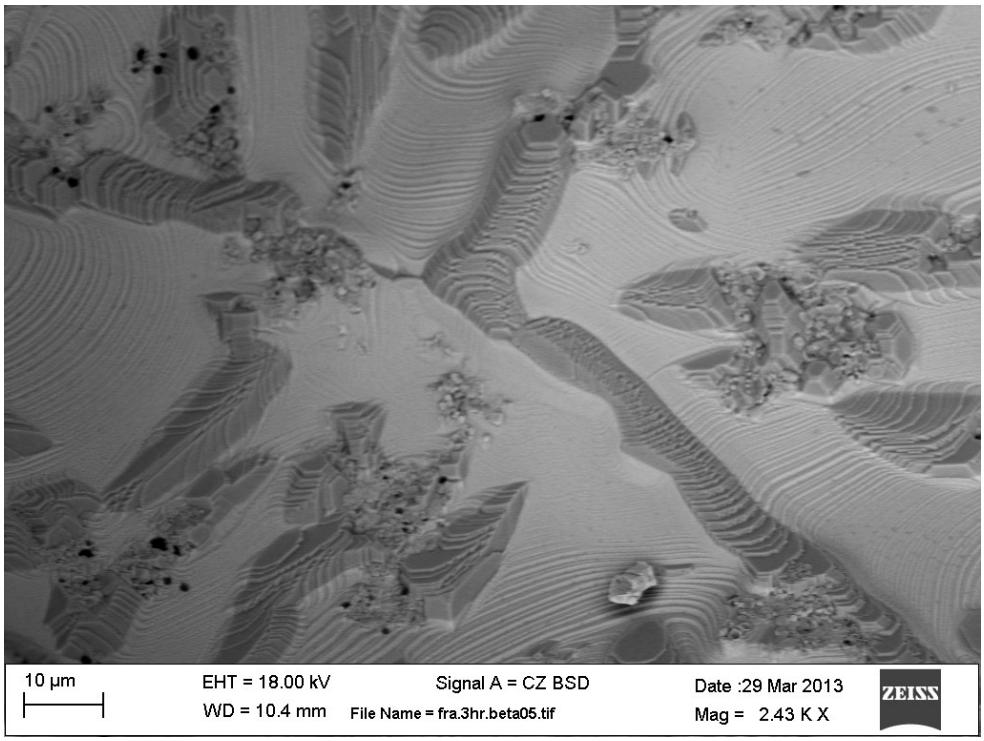

Figure 59: Scanning electron microscope image of 3-hour sample, 2.43 L X magnification. View of the inside of a large pore in the 3-hour sample.

In this area of the material, there are areas that are primarily silver telluride that are seamlessly joined with lead telluride. A large number of ledges are present that appear to cross uninterrupted from the lead telluride through the silver telluride and back to the lead telluride. Also present are large numbers of small, triangular silver telluride precipitates, as seen in Figure 60.

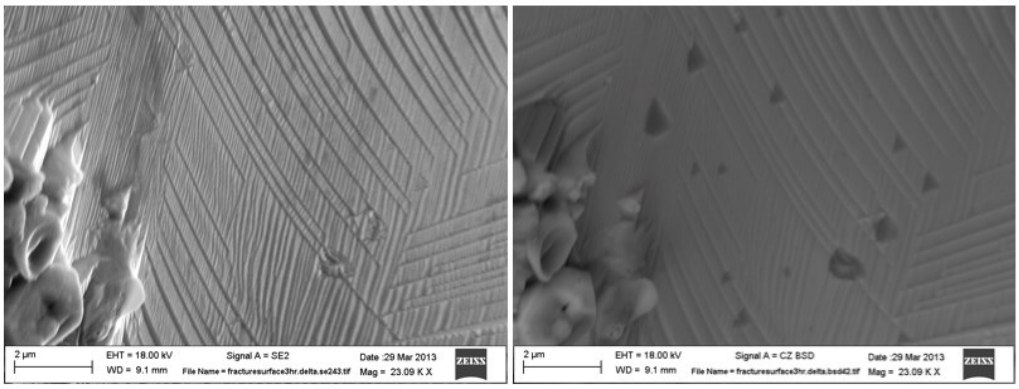

Figure 60: Precipitates in the 3-hour sample. SE2 (L.) and BSD (R.) images of silver telluride precipitates in a 3hr sample.

4.6. "Grid" Sample

In the research performed on the PbTe/Ag_2Te samples, it was difficult to locate the liquid phase because the contrast was very faint, even in BSD mode. This should be unsurprising, because there are so many variables involved with liquid phase sintering: grain rearrangement, grain growth, matter transport, liquid phase development, dissolution of the solute and precipitation of the solute to name a few. To further track the liquid formation and motion, an experiment was designed to reduce the number of variables involved. To do this, one sample was prepared through cold pressing with the same PbTe/Ag_2Te content as the others. Also, a large chunk of pure PbTe was placed on top of the pressed PbTe/Ag_2Te mixture, seen in figure 61.

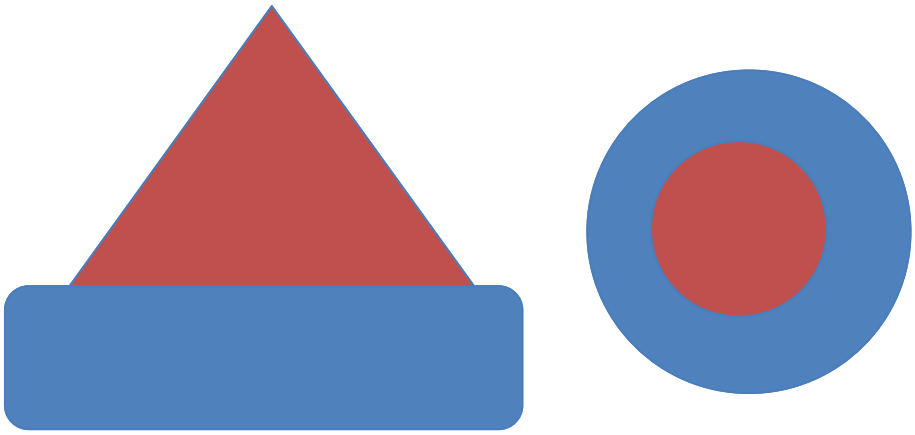

Figure 61: Schematic representation of "grid" sample setup. The blue is the pressed PbTe/Ag_2Te mixture, while the red is the pure PbTe, with the cross sectional on the left and top view on the right.

It was believed that this setup would give some control over how the sintering happened. The sample was sintered for one hour at 750°C, with the goal that the two pieces would fuse together. The pure PbTe would exist as one large grain, which would swallow the smaller grains of the PbTe/Ag_2Te mixture, allowing some control over the grain growth. We would then be able to view the region between the two with the SEM, and from the more controlled growth conditions be better able to track the liquid phase.

After the sample was sintered, it was polished, and then viewed under the SEM in backscattering mode with a wide view, the results seen in Figure 62.

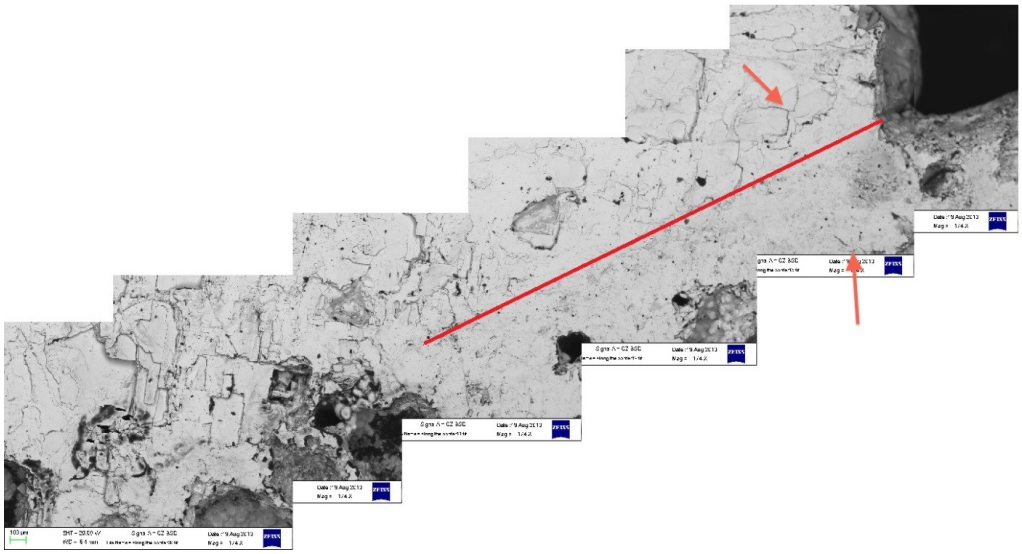

Figure 62: Border image between PbTe and Ag_2Te. This "stitched" image of several pictures of the border between the pressed PbTe/Ag_2Te mixture (below the red line) and the pure PbTe (above the red line). The arrows represent the region that was examined more closely, seen in Figure 63.

From this view of the border between the two parts of the sample, a section was chosen for closer examination. Since this was aiming to track how the liquid phase moved, a large area was chosen (between the two red arrows in Figure 62) and this area was looked at in a grid pattern at high magnification, 3.17 K, with the individual images overlapping. From there the images were "stitched" together, the results seen in Figure 63.

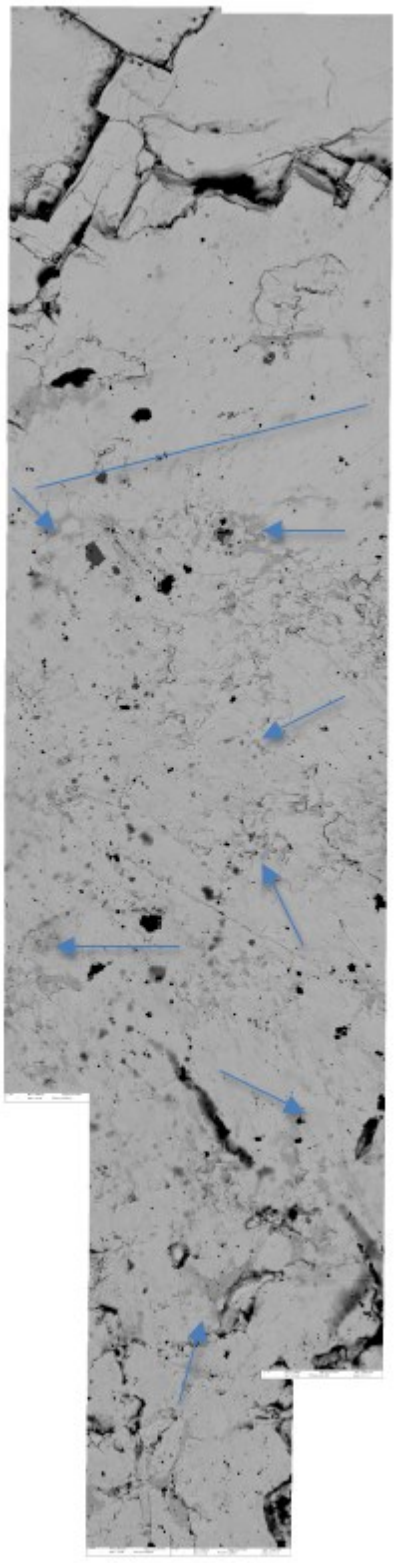

Figure 63: A view of the final product of "stitching" the individual micrographs. The blue line represents the probable border between the 2 parts of the sample. It can be seen that the liquid (the darker phase in the backscatter images) does not travel very far into the pure PbTe. The arrows highlight some of the frequent and widely distributed silver telluride "pockets" in the doped region of the sample, in contrast to how little silver telluride was found in the pure PbTe region of the sample

It can be seen that the amount of liquid phase varies throughout the sample. In the area below the line, that of the PbTe/Ag_2Te mixture, there is a large amount of silver telluride, randomly distributed throughout the sample, which is consistent with liquid phase sintering.

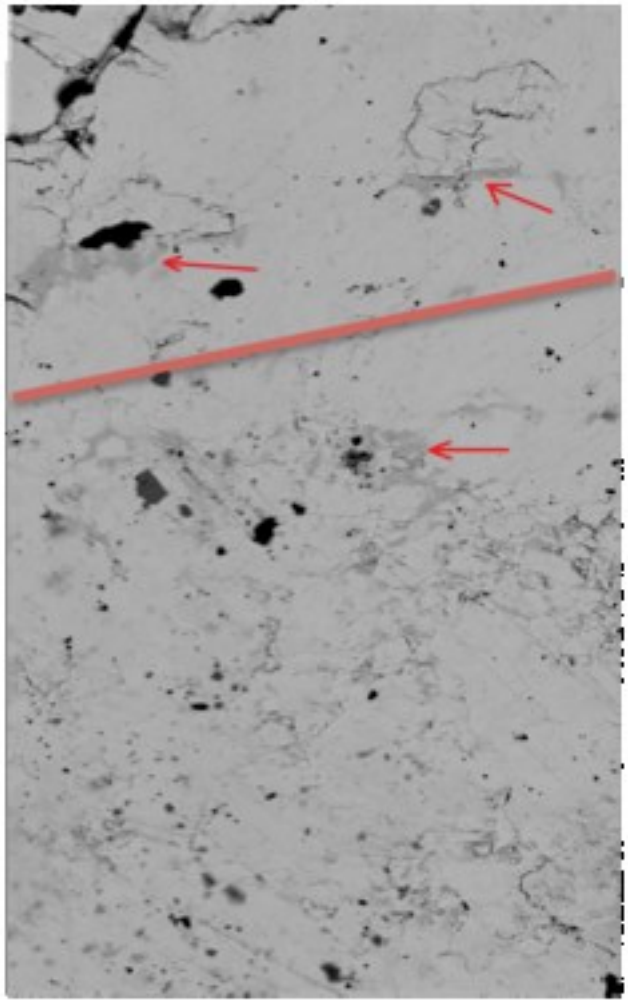

Figure 64: Close-up of the stitched image. The line represents the boundary between the two sections, and the arrows highlight various pockets of silver telluride within the sample.

A closer view shows more about the sample, and the movement of the liquid phase. The two top arrows show pockets of liquid that are trapped the zone that previously was pure PbTe. According to Rahaman [50] during Ostwald Ripening

during liquid phase sintering "smaller grains dissolve and precipitate on the larger grains." While this is happening, some of the liquid might be "trapped" by the grain growth. The bottom arrow shows a pocket that is within the PbTe/Ag_2Te mixture, and it is reminiscent of other micrographs seen in this system, with lacey tendrils and a random appearance. The region between the top and bottom arrows is the "recrystallization region" and is characterized by an absence of liquid. In this region, as the larger grains grew at the expense of smaller grains, and some of the liquid was trapped in this large grained region.

5. Discussion

This study of the liquid phase during the sintering of lead telluride reveals a complex process with significant advantages. When the undoped sample was sintered, a long sintering time lead to a sample that was still early in the sintering cycle. When Ag_2Te was introduced to the system as a sintering aid and the sintering temperature was raised slightly to ensure that it would melt it was found that sintering occurred at a much faster rate.

The samples that were sintered with Ag_2Te possessed several desirable characteristics. The seemingly improved particle packing was one, as denser ceramics typically have better electrical and mechanical properties. The shorter sintering time could help thermoelectrics become more industry friendly. The multiple phases revealed by the SEM backscatter detector and the EDS detector are also promising, because of their potential to scatter phonons and lower the thermal conductivity in the material. The structures seen in 60, which we believe

to be nano-precipitates, are especially promising because of the results seen in the literature for nano-precipitates for the PbTe/Ag_2Te system. These features develop as a result of the liquid-solid phase equilibrium condition that was stabilized during the high temperature heating and the slow cooling that follows. As seen in Figure 65, at 750°C there is both a liquid and a solid present, the liquid having more silver than the solid phase does.

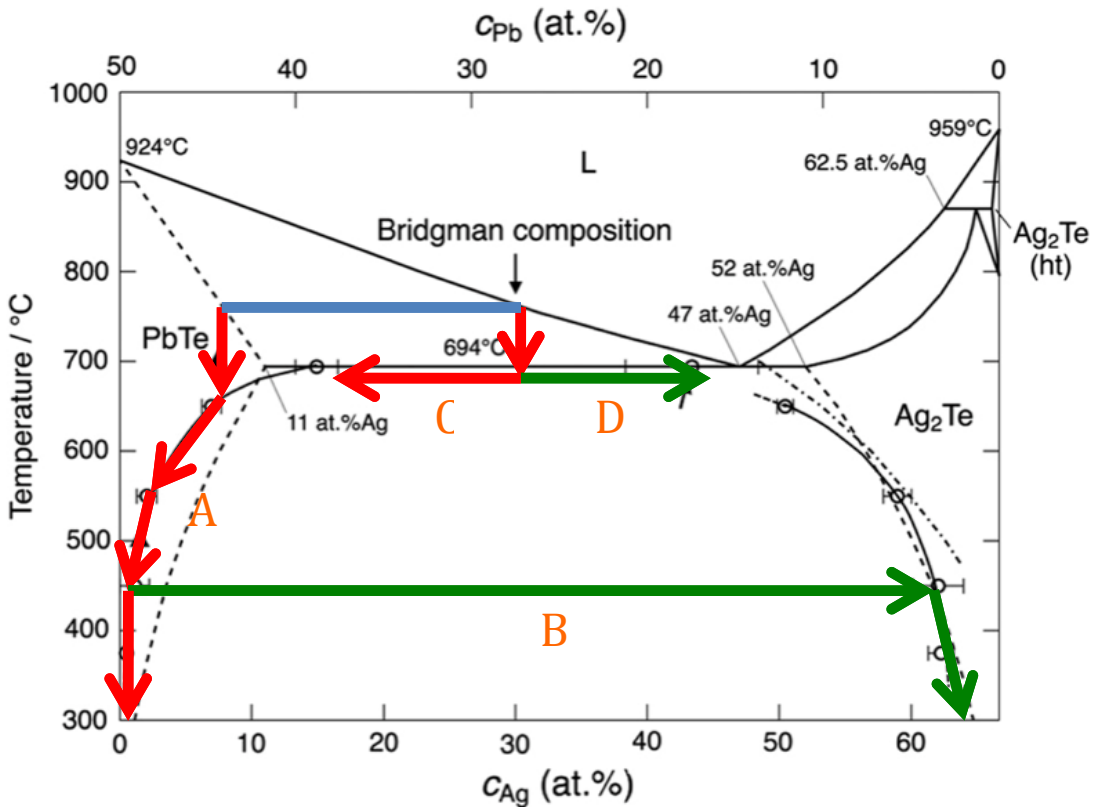

Figure 65: Phase diagram of PbTe/Ag_2Te showing how the microstructure evolves during cooling. The red arrows represent the lead telluride, and the green arrows represent the silver telluride. Letters are added for ease of reference, A for lead telluride from the solid, B for silver telluride from the solid, C for lead telluride from the liquid, and D for silver telluride from the liquid. Figure adopted from [12].

As the system cools, there are several processes that take place. As the solid cools, it is not able to have as much silver telluride (B) dissolved in it as it

would at high temperatures, so the silver telluride experiences internal nucleation, leading to some as the triangular shapes that were seen in Figure 60.

The liquid phase cools to the eutectic point and separates into lead telluride (C) and silver telluride (D) as it cools. Since the cooling happens slowly then the lead telluride can plate out onto the existing solid grains leaving behind the remaining silver telluride to precipitate on the surface. Lead telluride has the rocksalt structure, while below 140^{o}C silver telluride has a monoclinic structure [51] which is closely related to that of PbTe, which may account for the relatively continuous ledges going between the two phases with no discernable morphological change. In an open environment, such as inside a large pore, at high temperatures, the vapor and surface transport would be high, which could allow for low energy structural growth, leading to the lead telluride and silver telluride forming coherent structures.

While these characteristics are positive, this process is still in development. The products were unable to develop into fully dense ceramics; they either were without macroporosity but were highly porous on the micro-scale or they were less porous on the micro scale but contained macroporosity. This is most likely undesirable, and would need to be dealt with. Another more fundamental problem was the difficulty with tracking the liquid phase in the sample. This proved to be far more difficult than first envisioned. In the backscatter detector some contrast was evident, but it was not as sharp as some of the contrast that was found in the literature (see Figure 30). While we were able to identify small pockets of liquid in

the final polished cross-sections, it was not possible to measure dihedral angles or wetting of this liquid at the grain junctions.

While this study is ending, there are several things that could be done to continue it. Further work should be done on densifying the sample. This could be achieved by varying the amount of liquid generated during the heat treatment of the material. Also, better understanding is needed on the effect of inhomogeneous distribution of silver telluride after cold pressing on the sintering of the material. While this could be possibly be achieved through longer milling times, it would be difficult to quantify this. It would be valuable to see if a co-precipitation route toward the powder, one that possibly would form a powder where a layer of silver telluride surrounded each particle of lead telluride, would lead to better densification during sintering. This could be more quantifiable, because it would ensure an even distribution of the silver telluride. It is possible this could cut down on the wicking phenomenon by having the silver telluride better distributed. A narrower distribution of pore sizes could also cut down on this wicking effect, so a route towards better powder packing in the pressing stages should be examined as well.

Further work also needs to be done to better understand the liquid phase in the sample. A high temperature ceramic, such as ZrO_2 or Al_2O_3, in powder form could be added in to act as a "marker" to trace where the liquid was going. The thought behind the idea is that since these ceramics would not sinter at PbTe temperature, so they would not join with the solid particles. However, due to capillary action, if they were small enough they might move with the liquid. Then,

using SEM imaging and EDS, these particles could be tracked to provide more information about how the liquid moves in the sample. Several other more common techniques could also be used to provide more information about the liquid phase. Some work was done by the author using etches to try and discover the liquid phase, but was met with limited success. Nonetheless, this is a technique that should be pursued further. Also, more quenches should be looked at, to see if the liquid phase can be "frozen," and from it more information gleaned.

Though it was outside of the scope of this study, the thermoelectric properties of these materials must also be examined. The secondary phases and precipitates have the potential to be excellent at scattering phonons, and with proper doping these sample could potentially modify the electronic properties as well.

6. Conclusions

PbTe/Ag_2Te was studied in an attempt to develop a liquid phase sintering route towards dense, efficient thermoelectric materials. This process found mixed results. The PbTe/Ag_2Te samples appeared to sinter much faster than the PbTe sample, and had dense areas, both of which are desirable. However, there were also large, macroscopic pores in the PbTe/Ag_2Te samples. Furthermore, one of the main goals of this study was to track the liquid phase in the sample, which was also met with mixed results. While some contrast was found with the backscatter detector, and that contrast was identified with the EDS to be silver rich, true tracking of the liquid phase was not achieved.

This study had many promising aspects, and it is the belief of the author that the general program in PbTe sintering should be continued. The much improved rate of densification vs solid state sintering could provide an industry-friendly way of producing mass amounts of thermoelectrics in a short amount of time, with potentially desirable thermoelectric and mechanical properties. The silver telluride, which was partly dissolved into the grains, formed second phases including tiny intergranular precipitates that are promising for lowering thermal conductivity.

As conventional energy sources become increasingly problematic and more expensive, it is important to develop alternative methods to power our modern world. Thermoelectrics could help fill that role, particularly in the area of waste heat recovery. Thermoelectrics are not the "silver bullet" in the quest towards alternative energy, but in truth, this bullet is non-existent. By coming to rely so heavily on so few energy sources in the 20th century, humanity became vulnerable to losing its way of life one day as these sources become increasingly scarce. A diversified approach to energy policy, an approach that embraces solar, wind, and many other techniques, including thermoelectrics, could prevent this from happening again. Hopefully, through the continued study of thermoelectrics, this goal may be brought closer to fulfillment.

References

1. Z.H. Dughaish, "Lead Telluride as a Thermoelectric Material for Thermoelectric Power Generation," *Physica B*, **322** (2002), 205-223.

2. Cronin B. Vining, "An Inconvenient Truth About Thermoelectrics," *Nature Materials*, **8** (2009), 83-85

3. Yanzhong Pei, *et al.,* "High Thermoelectric Performance in PbTe Due to Large Nanoscale Ag_2Te Precipitates and La Doping," *Adv. Funct. Mater.,* **21** (2011) 241-249.

4. Heng Wang, *et al.,* "Reduction of Thermal Conductivity in PbTe:Tl by Alloying with $TlSbTe_2$" *Physical Review B,* **83** (2011) 024303-1 – 024303-5

5. Heng Wang, Jing-Feng Li, Takuji Kita, "Thermoelectric Enhancement at Low Temperature in Nonstoichiometric Lead-Telluride Compounds," *J. Phys. D: Appl. Phys.*, **40** (2007), 6839-6845.

6. Y Q Cao, T J Zhu, and X B Zhao, "Low Thermal Conductivity and Improved Figure of Merit in Fine-Grained Binary PbTe Thermoelectric Alloys," *J. Phys. D: Appl. Phys.*, **42** (2009), 015406-015611.

7. Christopher J. Vineis *et al.,* "Nanostructured Thermoelectrics: Big Efficiency Gains From Small Features," *Adv. Mater.,* **22** (2010), 3970-3980.

8. S. Gorsse et al., "Microstructure Engineering Design for Thermoelectric Materials: An Approach to Minimize Thermal Diffusivity," *Chem. Mater.*, **22** (2010), 988-993.

9. N. Bouad et al., "Mechanical Alloying of a Thermoelectric Alloy: $Pb_{0.65}Sn_{0.35}Te$," *J. of Solid State Chemistry*, **177** (2004), 221-226.

10. N. Bouad et al., "Phase Transformation Study of Pb-Te Powders During Mechanical Alloying," *Journal of Alloys and Compounds*, **353** (2003) 184-188.

11. P.N. Lim et al., "Synthesis and Processing of Nanostructured Thermoelectric Materials," *SIMTech Technical Reports,* **12** (2011), 98-104.

12. Kristin Bergum, Teruyuki Ikeda, and G. Jeffrey Snyder, "Solubility and Microstructure in the Pseudo-Binary PbTe-Ag_2Te System," *J. of Solid State Chemistry*, **184** (2011), 2543-2552.

13. Yanzhong Pei et al., "Combination of Large Nanostructures and Complex Band Structure for High Performance Thermoelectric Lead Telluride," *Energy Environ. Sci.*, **4** (2011), 3640-3645.

14. Julian H. Goldsmid, *Introduction to Thermoelectricity,* Springer, 2010.

15. C. Wood, "Materials for Thermoelectric Energy Conversion" *Rep. Prog. Phys.* **51** (1988) 459-539.

16. R.E. Newnham, *Properties of Materials: Anisotropy, Symmetry, Structure,* Oxford University Press, 2005.

17. Terry M. Tritt, and M.A Subramanian, "Thermoelectric Materials, Phenomena, and Applications: A Bird's Eye View," *MRS Bulletin* **31** (2006) 188-194

18. D.M. Rowe, "Chapter 1: General Principles and Basic Considerations," *Thermoelectrics Handbook: Macro to Nano*, Taylor and Francis, 2006.

19. Jonathan D'angelo, *et al.* "Electrical, Thermal, and Mechanical Characterization of Novel Segmented-Leg Thermoelectric Modules," *J. Electron. Mtrls.* **40** (2011) 2051-2062.

20. Kawamoto, Hiroshi, "R&D Trends in High Efficiency Thermoelectric Conversion Materials for Waste Heat Recovery," *Science and Technology Trends,* **30** (2009) 54-69.

21. David Emin "Chapter 5: Effects of Charge Carriers' Interactions on Seebeck Coefficients" *Thermoelectrics Handbook: Macro to Nano*, Taylor and Francis, 2006.

22. A.T. Burkov, "Chapter 22: Measurements of Resistivity and Thermopower: Principles and Practical Realization," *Thermoelectrics Handbook: Macro to Nano*, Taylor and Francis, 2006.

23. G. Jeffrey Snyder, and Eric S. Toberer, "Complex Thermoelectric Materials," *Nature Materials*, **7** (2008) 105-114.

24. Martin Wagner, *Simulation of Thermoelectric Devices,* http://www.iue.tuwien.ac.at/phd/mwagner/node49.html, 2007

25. Joesph P. Hermans, Christopher M. Thrush, and Donald T. Morelli, "Thermopower Enhancement in Lead Telluride Nanostructures," *Physical Review B,* **70** (2004) 115334-1 - 114334-5.

26. Kanishka Biswas, *et al*, "High-Performance Bulk Thermoelectrics with All-Scale Hierarchical Architectures," *Nature,* **489** (2012) 414-418.

27. Li-Dong Zhao, *et al.,* "Effect of Mixed Grain Sizes on Thermoelectric Performance of Bi_2Te_3 Compound," *J. of App. Physics,* **105** (2009) 023704-1 – 023704-6.

28. Jing Feng Li, *et al.,* "High-Performance Nanostructured Thermoelectric Materials," *NPG Asia Mater.* **2** (2010) 152-158.

29. Ju-Hyuk Kim, et al. "Effect of Composition on Thermoelectric Properties in PbTe-Bi_2Te_3 Composites," *Journal of Electronic Materials*, **40** (2011) 1010-1014.

30. Qiang Shen, Junguo Li, Lianment Zhang, "A Study on Sn Ion Implantation into Lead Telluride Thermoelectric Material," *Solar Energy Mat. and Solar Cells* **62** (2000) 167-172.

31. Kanishka Biswas et al., "High Thermoelectric Figure of Merit in Nanostructured p-Type PbTe-MTe (M = Ca, Ba)," *Energy Environ. Sci.,* **4** (2011), 4675-4684.

32. J.Q. Li, *et al,* "Effect of Ce-Doping on Thermoelectric Properties in PbTe Alloys Prepared by Spark Plasma Sintering" *J. Elect. Mat.,* **40** (2011) 2063-2068.

33. John Androulakis, *et al*., "Thermoelectric Enhancement in PbTe with K or Na Codoping from Tuning the Interaction of Light- and Heavy- Hole Valence Bands," *Phys. Rev. B,* **82** (2010) 115209-1 – 115209-8.

34. C. Chubilleau, *et al.,* "Laser Fragmentation in Liquid Medium: A New Way for the Synthesis of PbTe Nanoparticles," *J. of Coll. and Inter. Sci.* **357** (2011) 13-17.

35. Shreyashi Ganguly and Stephanie L. Brock, "Toward Nanostructured Thermoelectrics: Synthesis and Characterization of Lead Telluride Gels and Aerogels," *J. Mater. Chem.,* **21** (2011) 8800-8806.

36. M.N. Rahaman, *Ceramic Processing and Sintering,* Marcel Dekker, Inc., 1995.

37. Randall M. German, Pavan Suri, and Seong Jin Park, "Review: Liquid Phase Sintering" *J. Mater. Sci.,* **44**
(2009) 1-39.

38. Randall M. German, *Liquid Phase Sintering*, Plenum Press, 1985.

39. Kim, Ji Woo, *et.al.* "Synthesis of Liquid Phase Sintering of TiN/TiB_2/Fe-Cr-Ni Nanocomposite Powder," *J. of Alloys and Compounds*, **422** (2006) 62-66.

40. James H. Wittke, http://www4.nau.edu/microanalysis/Microprobe-SEM/Instrumentation.html, 2008.

41. Vernon- Parry, K.D., "Scanning Electron Microscopy: An Introduction," *III-Vs Review,* **13** (2000) 40-44.

42. Joseph Goldstein, *et al., Scanning Electron Microscopy and X-ray Microanalysis*, Springer, 2003.

43. "Physical Characterization," http://www3.nd.edu/~kamatlab/facilities_physchar.html.

44 Bob Hafner, "Energy Dispersive Spectroscopy on the SEM: A Primer," http://www.charfac.umn.edu/instruments/eds_on_sem_primer.pdf.

45. Yanzhong Pei, Andrew F. May, and G. Jeffrey Snyder, "Self-Tuning the Carrier Concentration of PbTe/Ag_2Te Composites with Excess Ag for High Thermoelectric Performance," *Advanced Energy Materials,* **1** (2011) 291-296.

46. Yanzhong Pei, Nicholas A. Heinz, and G. Jeffrey Snyder, "Alloying to Increase the Band Gap for Improving Thermoelectric Properties of Ag_2Te," *J. Mater. Chem*., **21** (2011) 18256-18260.

47 Yanzhong Pei, *et al..* "High Thermoelectric Figure of Merit in Heavy Hole Dominated PbTe" *Energy Environ. Sci.,* **4** (2011) 2085-2089.

48. N. Bouad, R.M. Marin-Ayral, J.C. Tedenac, "Mechanical Alloying and Sintering of Lead Telluride," *Journal of Alloys and Compounds,* **297** (2000) 312-318.

49. R. Breschi, and V. Fano, "The Sintering of Lead Telluride," *Journal of Materials Science,* **20** (1985) 2990-2996.

50. Thomas M. Shaw, "Model for the Effect of Powder Packing on the Driving Force for Liquid-Phase Sintering," *J. Am. Ceram. Soc.,* **76** (1993) 664-670.

51. J.L. Lensh-Falk et al., "Morphological Evolution of Ag_2Te Precipitates in Thermoelectric PbTe," *Journal of Alloys and Compound,* 504 (2010), 37-44.